NASA
Technical
Paper
3056

October 1990

Design of Control Laws for Flutter Suppression Based on the Aerodynamic Energy Concept and Comparisons With Other Design Methods

E. Nissim

NASA

NASA Technical Paper 3056

1990

Design of Control Laws for Flutter Suppression Based on the Aerodynamic Energy Concept and Comparisons With Other Design Methods

E. Nissim
Ames Research Center
Dryden Flight Research Facility
Edwards, California

National Aeronautics and Space Administration
Office of Management
Scientific and Technical Information Division

CONTENTS

SUMMARY

The aerodynamic energy method is used to synthesize control laws for NASA's drone for aerodynamic and structural testing–aerodynamic research wing 1 (DAST–ARW1) mathematical model. The performance of these control laws in terms of closed-loop flutter dynamic pressure, control surface activity, and robustness is compared with other control laws that appear in the literature and that relate to the same model. A control law synthesis technique that makes use of the return difference singular values is developed in the present work. It is based on the aerodynamic energy approach and is shown to yield results that are superior to those results given in the literature and are based on optimal control theory. Nyquist plots are presented, together with a short discussion regarding the relative merits of the minimum singular value as a measure of robustness as compared with the more traditional measure involving phase and gain margins.

INTRODUCTION

In recent years, a considerable amount of work has been done in the field of flutter suppression using active controls (Gangsaas and Uy-Loi, 1979; Mahesh et al., 1979; Mahesh et al., 1981; Mukhopadhyay, 1987; Mukhopadhyay et al., 1981, 1982; Mukhopadhyay and Newsom,1982; Newsom, 1979; Newsom et al., 1983). The common denominator for most of these works is that they are based on optimal control theory. This requires the formulation of the aeroservoelastic equations in state–space form that results in equations involving many states. A realistic design, for example, with 10 structural modes, may lead to equations with approximately 60–70 states associated partly with the structural modes and actuator dynamics, and partly with the augmented states caused by the aerodynamic lag terms representation.

Optimal control theory, based on the standard linear quadratic Gaussian (LQG) solution, yields an optimal feedback control law of the same high order as the plant. Also, this optimal control law is invariably sensitive to modeling errors, has poor stability margins, and is often too complex to implement in a flight computer because of its high order. The robustness of the optimal control law based on the LQG design techniques can be considerably improved (Doyle and Stein, 1979) by introducing a fictitious input noise. However, the resulting LQG controller remains the same high order as the plant. Also, the minimization of the performance index involving the plant states cannot be readily related to the root mean square (rms) responses, since these former responses contain fictitious noise effects introduced into the system. As a result, a multitude of methods have been suggested for both reducing the order of the resulting control law and for maintaining the robustness improvement obtained by the introduction of fictitious noise.

Methods suggested for obtaining reduced order control laws are derived using optimal control theory with truncation (Gangsaas and Uy-Loi, 1979; Mukhopadhyay et al., 1981), residualization (Mahesh et al., 1979), or transfer function matching (Newsom, 1979) methods. In the truncation method (Gangsaas and Uy-Loi, 1979), the low-order controller is obtained by partitioning the optimal full-state feedback and Kalman estimator gain matrices and retaining only the optimal controller part corresponding to the key states and their first derivatives. Reoptimizing the preceding truncated control law using a numerical optimization algorithm (Mukhopadhyay et al., 1981), together with the improved robustness method using fictitious input noise, yields improved results (compared with the unoptimized truncation results using no fictitious noise). In the residualization method (Mahesh et al., 1979), a first-order correction is added to the truncation method (Gangsaas and Uy-Loi, 1979) by retaining the static part of the controller corresponding to the rest of the states. In the transfer-function matching method (Newsom, 1979), the optimal high-order control law is approximated by a low-order control law, the order of which is arbitrarily determined. The parameters of the assumed low-order control law are determined using an optimization algorithm that minimizes the deviations from the optimal control law over a range of frequencies.

The main virtue of the optimal control theory is in providing tools for synthesizing control laws that stabilize the system using full-order controllers. These control laws clearly depend on the relative values of the different

matrix elements *assumed* while formulating the performance index, the level of input noise (if any) introduced, the final order of the desired control law, and the method chosen for the control law order reduction. Also, the more potent of the previously mentioned design methods (Mukhopadhyay et al., 1981; Newsom, 1979) require numerical optimization techniques to achieve the final control law. Therefore, the design of a control law involves a long process by which arbitrary parameters (like those assumed in the performance index) are varied, and the resulting control law's performance is tested and compared with the desired performance.

The aerodynamic energy approach (Nissim, 1971, 1977, 1978; Nissim and Abel, 1978; Nissim and Lottati, 1980; Nissim et al., 1976) permits the stabilization of fluttering systems in a manner insensitive to flight conditions, mode shapes, and so forth, while using low-order control laws. Robust, low-order control laws form the basis of the aerodynamic energy synthesis technique. Its potency could be readily improved and its performance evaluated and compared with other design techniques based on optimum control theory. This latter comparison is the prime objective of the report.

The report contains a brief review of the aerodynamic energy concept, together with the most important results obtained to date. Different control law design techniques, based on the aerodynamic energy concept, are evaluated. The results are compared with those based on optimal control theory. Finally, an evaluation of the aerodynamic energy control law design technique is presented.

NOMENCLATURE

Abbreviations

DAST–ARW1	drone for aerodynamic and structural testing–aerodynamic research wing 1
DTTF	damping-type transfer function
LDTTF	localized damping-type transfer function
L.E.	leading edge
LQG	linear quadratic Gaussian
MSV	minimum singular value
rms	root mean square
SISO	single input–single output
T.E.	trailing edge

Letter and Mathematical Symbols

a_L, a_T	positive gains
b	semichord length at the sensor's section
c	reference chord
G, H	matrices in open-loop transfer function
g	gravitational acceleration
h	plunge displacement, positive down
h_s	plunge displacement of sensor
M	Mach number
Q	dynamic pressure

Q_D	design dynamic pressure
Q_F	flutter dynamic pressure
R_u	fictitious input–noise intensity matrix
S_F	transfer function of structural filter
s	the Laplace transform
W	work done on surrounding per cycle of oscillation
W_s	weighting scalar defined in equation (13)
α	torsional angle, positive nose up
β	leading-edge deflection, positive nose down
γ	variable defined in equation (15)
δ	trailing-edge deflection, positive tail down
δ_c	rotational command for trailing-edge deflection
ζ	damping coefficient
λ	aerodynamic eigenvalue
σ	singular value of return difference
$\underline{\sigma}$	minimum singular value of return difference
$\underline{\sigma}_D$	desired minimum singular value
ω	frequency of oscillation
ω_n	natural frequency of second-order pole

Subscripts

F	flutter
inb	inboard driving sensor
L	leading-edge control
max	largest
min	smallest
$outb$	outboard driving sensor
T	trailing-edge control

REVIEW OF AERODYNAMIC ENERGY CONCEPT

General Approach

The aerodynamic energy concept uses the work W done by the system on its surrounding per cycle of oscillation as a basis for determining the system's stability. If the system does positive work per cycle of oscillation ($W > 0$), the system is dissipating energy and is stable. But, if the system does negative work per cycle of oscillation ($W < 0$), the system is absorbing energy and is unstable. At flutter, no exchange of energy takes place because the system is neutrally stable, and therefore $W = 0$.

The mathematical expression developed (Nissim, 1971, 1977) to evaluate W shows that the aircraft's inertial and elastic forces have no contributions to W, except for control surface mass unbalance inertial forces where control surfaces are left unbalanced. When control surfaces are left unbalanced, the aerodynamic forces are the sole contributors to the energy exchange per cycle of oscillation. This result is not surprising because it is well known that dynamic systems involving only symmetrical mass and stiffness matrices always oscillate in neutral equilibrium and can never diverge in an oscillatory manner. Therefore, any flutter suppression effects from active controls are obtained by way of aerodynamic matrix changes made to the aerodynamic matrices using control surface aerodynamic contributions. In Nissim (1971, 1977), the expression for W is further reduced to a principal quadratic form involving quadratic coefficients and the square of the responses only (without cross products of responses). If these quadratic coefficients (denoted by λ's in Nissim (1971, 1977) and defined as aerodynamic eigenvalues) can be modified by an appropriate control law so that all become positive, then the system must be stable and dissipative. The square of the responses are always positive, thus yielding positive values for W regardless of the specific value of the responses.

In an attempt to obtain general results and avoid treating specific systems, the λ's representing the previously mentioned coefficients for the principal quadratic expression for W were computed numerically (Nissim, 1971, 1977) for a two-dimensional wing strip. Their values were modified through the use of generalized control laws to render all the λ's positive over a wide range of reduced frequencies and Mach numbers. The two-dimensional strip was allowed to plunge and pitch, and two control surfaces were permitted to be activated—a leading-edge (L.E.) and a trailing-edge (T.E.) control surface—each spanning 20 percent of the chord. The principal quadratic expression for W involves only two coefficients; that is, two λ's. The smallest of these two λ's is referred to as λ_{min} and the largest is referred to as λ_{max}. The results obtained for the two-dimensional wing can be applied to the three-dimensional wings based on the following assumptions: The basic motion of each strip in the three-dimensional wing must involve plunge and pitch motions, and the *ratios* between the different aerodynamic forces acting on the three-dimensional strip must be the same as the ratios for the two-dimensional strip (much the same way as in Glauert's lifting line theory). The main results pertaining to the two-dimensional strip (Nissim, 1971, 1977) are presented in the following section.

Review of Aerodynamic Energy Two-Dimensional Strip Results

The main results produced by the aerodynamic energy concept (Nissim, 1971, 1977) are summarized by the following points:

1. An L.E. alone has very little effect on either λ_{min} or λ_{max}.

2. A T.E. alone has little effect on λ_{min} and a large effect on λ_{max}. With a proper control law, λ_{max} can be made very large and positive, while λ_{min} is generally negative but can be brought to approach zero.

3. An L.E.–T.E. system greatly affects both λ_{min} and λ_{max}, with λ_{min} affected largely by the L.E. and λ_{max} affected largely by the T.E. Both λ_{min} and λ_{max} can be made positive and assume large values.

4. The most effective location on the strip for a single sensor activating the T.E. control is around the 65–70-percent chord location, with a slight variation with subsonic Mach number used.

5. The most effective location within the strip for a single sensor activating the L.E. control is around the −20-percent chord location (20-percent chord ahead of the strip's L.E.). Since this location is impractical for a single sensor, two sensors need to be used to project the motion to the −20-percent chord location.

6. Denoting the motion of the T.E. and L.E. sensors located as described in items 4 and 5 by $h_{s,T}$ and $h_{s,L}$, respectively, the most effective control law for all control systems (that is, T.E. alone and combined L.E.–T.E. systems) is where the T.E. control deflection is in phase with the velocity of its driving sensor ($\dot{h}_{s,T}$), and the L.E. control deflection is in antiphase with the velocity of its driving sensor ($-\dot{h}_{s,L}$).

Review of Specific Control Laws Obtained Using the Aerodynamic Energy Concept

Using the notation presented in the following sketch, with h denoting the plunge displacement at the 30-percent chord location and with the arrows denoting the positive displacement and rotations, the fundamental aerodynamic

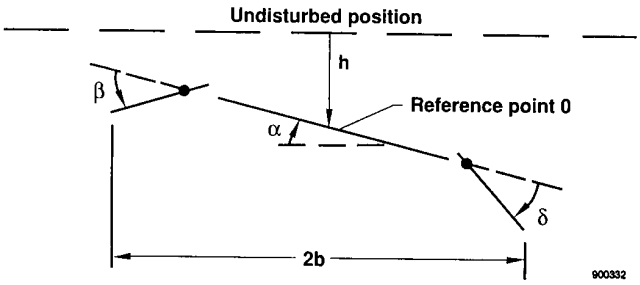

energy control law derived in Nissim (1977), and denoted as the damping-type transfer function (DTTF), is given by the following expression

$$\begin{Bmatrix} \beta \\ \delta \end{Bmatrix} = \begin{bmatrix} 0. & 0. \\ 0. & -1.86 \end{bmatrix} \begin{Bmatrix} h/b \\ \alpha \end{Bmatrix} + \begin{bmatrix} a_L & \\ & a_T \end{bmatrix} \begin{bmatrix} -4 & 4 \\ 4 & 3.2 \end{bmatrix} \begin{Bmatrix} \dot{h}/b \\ \dot{\alpha} \end{Bmatrix} \tag{1}$$

where a_L and a_T are *positive* gains (or zero) determined while designing a specific system. For a T.E. alone system, $a_L = 0$ and only the equation associated with δ need be considered. Also, when the gains a_L and a_T are sufficiently large, the matrix associated with the displacements can be discarded. These coefficients affect the λ's very slightly, and use of the following simplified control law can be made:

$$\begin{Bmatrix} \beta \\ \delta \end{Bmatrix} = \begin{bmatrix} a_L & \\ & a_T \end{bmatrix} \begin{bmatrix} -4 & 4 \\ 4 & 3.2 \end{bmatrix} \begin{Bmatrix} \dot{h}/b \\ \dot{\alpha} \end{Bmatrix} \tag{2}$$

Equation (2) forms the basis for the results presented in the previous section under points 4, 5, and 6. Note that by placing the sensors at the locations described in points 4 and 5, the ratios between the two numerical columns in equation (2) are maintained. These ratios are important since multiplying factors can be lumped with the constants a_L and a_T (Nissim, 1977). The control law presented in equation (2) is of a basic nature and is shown to be approximated by the different robust control laws derived by a variety of design methods. However, this control law is impractical in its present form since it does not permit the introduction of damping over a limited range of frequencies. Instead, damping is introduced over an uncontrolled range of frequencies, with possible penalties paid in terms of unnecessary control surface activity.

Also, equation (2) is impractical when considering the effects of actuator dynamics. The energy approach does not rule out the use of aerodynamic stiffness terms to change the response of the system for increase of responses associated with λ_{max}. Thus the system is made more dissipative. This is true for a T.E. alone control system where λ_{min} is small and not necessarily positive. Aerodynamic stiffness terms can be introduced through the terms proportional to the displacements, as in equation (1). These arguments led to the formulation of the localized damping-type

transfer function (LDTTF) (Nissim, 1977) summarized by the following control law that is a counterpart to the control law presented in equation (2):

$$\begin{Bmatrix} \beta \\ \delta \end{Bmatrix} = \begin{bmatrix} \dfrac{a_L s^2}{s^2 + 2\omega_{n,L}\zeta_L s + \omega_{n,L}^2} & \\ & \dfrac{a_T s^2}{s^2 + 2\omega_{n,T}\zeta_T s + \omega_{n,T}^2} \end{bmatrix} \begin{bmatrix} -4 & 4 \\ 4 & 2.8 \end{bmatrix} \begin{Bmatrix} h/b \\ \alpha \end{Bmatrix} \tag{3}$$

Again, a_L and a_T are positive gains, and s is the Laplace variable. The second-order transfer functions in the diagonal matrix in equation (3) yield terms proportional to s at resonance (that is, $s = i\omega_{n,L}$ or $s = i\omega_{n,T}$). Or, in other words, these functions yield control surface deflections in phase and antiphase with the rates of sensor displacements at the locations specified in points 4 and 5, much in accordance with the DTTF presented by equation (2). When at frequencies smaller or larger than the resonance frequencies of the second-order poles, these transfer functions also have real components (in quadrature with the velocity), and lead to aerodynamic stiffness terms in addition to the aerodynamic damping terms. The maximum amount of aerodynamic damping is introduced around the resonance frequencies of the second-order poles. These frequencies must be assigned numerical values around the flutter frequency. However, before summarizing the design procedure based on the foregoing results, it is stressed that the LDTTF is *only one of the many transfer functions* that can produce control deflections with large components in phase with $\dot{h}_{s,T}$ and in antiphase with $\dot{h}_{s,L}$ over a wide frequency range spanning the flutter frequency. Thus the fundamental results are presented by equation (2); that is, by the DTTF. *Practical implementations can assume a very wide variety of forms*, only one of which is given by the LDTTF. Additional examples of transfer functions yielding large components of control deflections in quadrature with the amplitudes of oscillation, as warranted by equation (2), are obtained by multiplying the LDTTF by lead–lag terms, or by considering the washout-type transfer function of the form $s/(s+a)$. In the following section, the design procedure developed in Nissim and Abel (1978), based on the LDTTF, is briefly presented. It is followed by the synthesis of control laws based on the foregoing results and on new techniques using a specific flutter example that includes actuator dynamics.

Review of Control Law Synthesis Technique

The idea behind the design technique developed in Nissim and Abel (1978) is to come up with a design that not only meets the stability requirements, but also yields minimum control surface activity. This is achieved by minimizing the response of the control surfaces to a gust input. In this manner the gust becomes a driver in establishing the closed-loop parameters, while maintaining stability and minimizing control surface RMS activity. The design procedure involves the following steps:

1. Choose initial values for the free parameters (a's, ω_n's, and ζ's) in the LDTTF that stabilize the system.

2. Minimize the control activity by optimizing the free parameters at the highest desired dynamic pressure and the highest subsonic Mach number, while constraining $\omega_{n,L}$ and $\omega_{n,T}$ to lie between 0.65 ω_F and 1.45 ω_F where ω_F denotes the flutter frequency.

3. Determine control surface activity over a range of flight conditions (lower Mach number and lower dynamic pressures, and possibly other flight configurations). If considerable increase in control surface activity is observed, repeat step 2 with a narrowed range for $\omega_{n,L}$ and $\omega_{n,T}$.

The constraints on the values of $\omega_{n,L}$ and $\omega_{n,T}$ are intended to ensure that stabilization is achieved by changing the λ's, thus assuring robustness irrespective of the responses. Changing the responses of the system with little effect on the λ's may make it sensitive to changes in responses brought about by small changes in flight conditions or by small modeling errors.

DAST–ARW1 MODEL

The objective of this work is to evaluate the aerodynamic energy design method by comparing the performance of its resulting control laws against those obtained by other methods based on the different forms of the optimal control theory. The mathematical model for NASA's drone for aerodynamic and structural testing–aerodynamic research wing 1 (DAST–ARW1) was chosen for this purpose because it served as a basis for the development of the different design techniques based on the optimal control theory. However, the complete mathematical model was no longer available. It had to be reconstructed using generalized mass and stiffness matrices, together with the mode shapes associated with the model's different degrees of freedom. The aerodynamic matrices were computed using the available mode shapes supplied by NASA. Therefore, the first step in the present work is to validate the model against the published results for the open- and closed-loop systems, bearing in mind that some variations might exist as a result of possible differences in the aircraft's aerodynamic modeling.

Description

The DAST–ARW1 model (Newsom et al., 1980) is a dynamically scaled representation of a transport-type research wing and was scaled to flutter within the operational limits of the Langley Transonic Dynamics Tunnel. The model was equipped with a hydraulically actuated T.E. control surface located between the 76.3 percent and 89.3 percent semispan stations. Its chord measured 20 percent of the local wing chord. The model's geometry is given in figure 1.

The mathematical model used for the aeroelastic analysis and aeroservoelastic synthesis comprises 10 elastic symmetrical modes. Its natural frequencies span the range of 5.23 to 118.15 Hz.

The unsteady aerodynamic forces for the wing and control surface were computed at Mach 0.9 for different values of reduced frequencies using doublet lattice aerodynamics. Unsteady aerodynamic forces were calculated for the 10 structural modes, the control surface rotation, and a sinusoidal gust.

The T.E. control surface, driven by an electrohydraulic servoactuator, was capable of approximately $\pm 14°$ rotation with rates of up to 820 deg/sec. The actuator transfer function is given by

$$\frac{\delta}{\delta_c} = \frac{1.915 \times 10^7}{(s + 214)(s^2 + 179.4s + 8.945 \times 10^4)} \text{ deg/deg} \tag{4}$$

where δ_c denotes the rotational command.

Validation

Newsom et al. (1980) form the basis for most of the comparisons between the present and the previously published performances. A more limited use is made of the results published in Mukhopadhyay et al. (1981). Most of these latter results relate to reduced-order systems while attempting to synthesize relatively low-order control laws.

Figures 2 and 3 compare the root locus plots of the open-loop system. The plots are identical, except for a small difference in the flutter dynamic pressure (Q_F), with Newsom et al. (1980) yielding $Q_F = 105$ lb/ft^2 compared with $Q_F = 99$ lb/ft^2 obtained here. There is also a small difference between the flutter frequencies (ω_F), with Newsom et al. (1980) yielding $\omega_F = 51.6$ rad/sec compared with $\omega_F = 50$ rad/sec obtained here.

For the closed-loop system, comparisons are made between the closed-loop values of Q_F and ω_F, Nyquist plots, stability margins, and control surface activities.

Figure 4 shows the closed-loop root locus plot obtained using the current model and the control law given in Newsom et al. (1980) by equation (9); that is

$$\frac{\delta_c}{\ddot{h}_{outb}} = \frac{2214}{(s+10)}\frac{s}{(s+1)}\left[\frac{s^2+30.79s+14{,}692}{s^2+572.6s+88{,}578}\right]\left[\frac{s^2+47.37s+72{,}436}{s^2+568.6s+86{,}972}\right]\frac{\text{deg}}{g} \tag{5}$$

where $\ddot{h}_{outb}$ refers to the accelerometer output located outboard of the T.E. control at the 60-percent chord location (fig. 1). In addition, a structural filter was added to the actuator in Newsom et al. (1980) to attenuate the high frequencies. This filter is denoted by S_F and is given by

$$S_F = \frac{(628)^2}{(s+628)^2} \tag{6}$$

Figure 5 shows the closed-loop root locus plot reproduced from Newsom et al. (1980). Note that figures 4 and 5 are similar, with the present work yielding $Q_F = 174$ lb/ft^2 and $\omega_F = 49$ rad/sec compared with the values of $Q_F = 188$ lb/ft^2 and $\omega_F = 44$ rad/sec given by Newsom et al. (1980). The percentage differences between the values of Q_F obtained in this report and those obtained in Newsom et al. (1980) are approximately the same for both the open-loop and closed-loop cases.

The design point in Newsom et al. (1980) relates to a dynamic pressure of 44 percent above the open-loop flutter dynamic pressure. Since $Q_F = 105$ lb/ft^2 in Newsom et al. (1980), the design dynamic pressure, denoted by Q_D, was assigned the value of $Q_D = 151$ lb/ft^2. However, since $Q_F = 99$ lb/ft^2 in the present work, the design dynamic pressure was 44 percent above this value, yielding $Q_D = 142.6$ lb/ft^2. Figures 6 and 7 show a comparison between the Nyquist plots obtained in this report and in Newsom et al. (1980). These figures are very similar, with figure 6 relating to the results obtained in the present work and yielding gain margins of -5.34 dB and 14.3 dB, compared with -6.0 dB and 16.5 dB obtained in Newsom et al. (1980). Similarly, the phase margins obtained are given by $-48°$ and 47°, compared with the Newsom et al. (1980) values of $-52°$ and 52°. The minimum singular value (MSV) of the return difference computed in this work is equal to MSV = 0.61. Because Newsom et al. (1980) does not present any values of the MSV's, these values were extracted graphically from the Nyquist plots (explained in detail later in the report), yielding for this case the value of MSV = 0.64. All of the results, together with results pertaining to control surface activities and additional results presented in the following sections, are summarized in table 1.

A comparison is also made between the results obtained in this report and those reported in Mukhopadhyay et al. (1981), using their control law, in equation (30):

$$\frac{\delta_c}{\ddot{h}_{outb}} = \frac{1939.4(s+24.74)(s^2+87.63s+13{,}806)}{(s+3.864)(s+3270)(s^2+20.97s+1423)}\frac{\text{deg}}{g} \tag{7}$$

The same actuator used in Newsom et al. (1980) was also used in this case. However, *no use* was made of the structural filter given by equation (6). In this instance, the design point in Mukhopadhyay et al. (1981) was chosen to be at $Q_D = 160$ lb/ft^2. Considering the differences between Newsom et al. (1980), Mukhopadhyay et al. (1981), and the present work regarding the open-loop flutter dynamic pressures, the equivalent value of Q_D for comparison purposes is $Q_D = 151$ lb/ft^2 ($= 160 \times \frac{99}{105}$). The results pertaining to the control law given by equation (7) (or eq. (30), Mukhopadhyay et al. (1981)), are summarized in table 1 and shown in figures 8–11. Note that there is good agreement between the results computed here and those reported in Mukhopadhyay et al. (1981).

Since these results form the basis for comparisons with the control laws derived in this report, mention is made of the methods employed for synthesis of these control laws. The control laws derived in Newsom et al. (1980) are based on optimal control theory, followed by control law order reduction using transfer-function matching leading to a sixth-order control law.

The control law derived in Mukhopadhyay et al. (1981) used a reduced-order model for the DAST–ARW1, yielding a 25th-order plant instead of the original 65th-order plant (full order). Also, truncation and reoptimization were used to derive the control law, together with the addition of fictitious noise at the input to improve robustness. Finally, the reduced-order control law thus obtained was evaluated using the full-order model of the plant.

DEVELOPMENT AND EVALUATION OF IMPROVED CONTROL LAW SYNTHESIS TECHNIQUE

In the following, control laws are synthesized in three cases. In the first case, actuator dynamics *are* ignored, and a procedure is developed to replace the relatively loose optimization constraints imposed on $\omega_{n,T}$ by a more definite requirement, such as the increase of the minimum singular value over a wide range of frequencies. The manifestation of the MSV on the Nyquist plots and its relation to phase and gain margins is studied to define an improved-design procedure. In the second case, actuator dynamics are introduced, together with the structural filter, using the design procedure defined in the first case. The results obtained in the second case are compared with those given in Newsom et al. (1980) and presented in table 1. In the third and final case, actuator dynamics are considered. However, the structural filter introduced in Newsom et al. (1980) is ignored, much the same as in Mukhopadhyay et al. (1981). The results obtained during the third case are compared with those given in Mukhopadhyay et al. (1981) and summarized in table 1. In all three cases, control laws are synthesized using the outboard accelerometer. The results are compared with the equivalent control laws synthesized using the inboard accelerometer that is warranted by the aerodynamic energy approach. Finally, the results obtained by the aerodynamic energy approach are evaluated and conclusions are drawn.

Case 1—Synthesis Technique and Presentation of Results for Systems With No Actuator Dynamics

As stated earlier, the DAST–ARW1 mathematical model consists of a wing with only a T.E. control surface. Thus, equation (3) can be simplified and brought to the form

$$\delta = \frac{4\,a_T s^2}{s^2 + 2\omega_{n,T}\zeta_T s + \omega_{n,T}^2}\left(\frac{h}{b} + 0.7\alpha\right) \tag{8}$$

Because h relates to the 30-percent chord point, the expression $(h + 0.7\,b\alpha)$ relates to a point at the 65-percent chord location. Therefore, equation (8) can be written as

$$\delta = \frac{4\,a_T s^2}{s^2 + 2\omega_{n,T}\zeta_T s + \omega_{n,T}^2}\frac{h_{0.65c}}{b} \tag{9}$$

or

$$\delta = \frac{4\,a_T s^2}{s^2 + 2\omega_{n,T}\zeta_T s + \omega_{n,T}^2}\frac{h_{inb}}{b} \tag{10}$$

Equation (10) is valid for the inboard accelerometer mentioned earlier. For the outboard accelerometer located on the 60-percent chord point, this location can be written by

$$h_{0.6c} = h_{0.3c} + 0.6\,b\alpha \tag{11}$$

Equation (11) leads to an equation similar to the one given by equation (3), but with the value of 2.8 replaced by 2.4 (0.6×4). This is a suboptimal location because of the change in value and the sensor's location just outside the

strip containing the T.E. control surface, instead of along its center span (fig. 1). For the outboard accelerometer, the following expression is used:

$$\delta = \frac{4\,a_T s^2}{s^2 + 2\omega_{n,T}\zeta_T s + \omega_{n,T}^2}\,\frac{h_{0.6c}}{b} \tag{12}$$

or

$$\delta = \frac{4\,a_T s^2}{s^2 + 2\omega_{n,T}\zeta_T s + \omega_{n,T}^2}\,\frac{h_{outb}}{b} \tag{13}$$

Following the aerodynamic energy control law synthesis procedure, the values of a_T, $\omega_{n,T}$, and ζ_T are evaluated both for the inboard and the outboard accelerometers. The target function used involves the rms value of the rate of the control surface response $\dot{\delta}_{\text{rms}}$ to a 1-ft/sec gust input. A compounded target function can be defined that also includes the control rms response in addition to the control rms rate; however, this possibility was not used. The Von-Karman gust spectrum is used throughout this report, with a characteristic length of 100 ft, to simulate the distribution and intensity of turbulence.

All the results obtained during case 1 are summarized in table 2 and the control laws are presented in appendixes A and B. Appendix A relates to control laws prefixed by the letter A and synthesized while using the inboard accelerometer as a driving sensor. Appendix B relates to equivalent control laws prefixed by the letter B and synthesized while using the outboard accelerometer as a driving sensor.

The first optimization runs were intended to test the effects of the optimization constraints imposed on $\omega_{n,T}$. To show the effects of the constraints on $\omega_{n,T}$, the value of $\omega_{n,T}$ was constrained to lie within the range $2 \leq \omega_{n,T} \leq 70$ rad/sec. In the second example, $\omega_{n,T}$ was constrained to lie within a narrower range defined by $35 \leq \omega_{n,T} \leq 70$ rad/sec with the aerodynamic energy synthesis technique. Note that only the lower bound was changed, since it is this bound that produces an active constraint.

Control laws A1 and B1 relate to the case where $\omega_{n,T}$ is permitted to go as far down as $\omega_{n,T} = 2$, where it hits the constraint. With $\omega_{n,T} = 2$ rad/sec and with the flutter frequency $\omega_F = 50$ rad/sec, it is unrealistic to expect large components (approximately the flutter frequency) of control surface deflections that are in phase with the velocity of the T.E. driving sensor. Therefore, although the control surface rates yield $\dot{\delta}_{\text{rms}}$ values of approximately 174 deg/sec, the phase margins obtained are poor (approximately 20° to 24°). The MSV's obtained assume the values of 0.31 for the outboard accelerometer and 0.35 for the inboard accelerometer. At this stage the design procedure based on the aerodynamic energy concept, as presented in Nissim and Abel (1978) and described earlier in this report (see point 2 of the reviewed synthesis technique), does not permit such a wide deviation of $\omega_{n,T}$ from the flutter frequency.

Control laws A2 and B2 relate to the case where the lower bound of $\omega_{n,T}$ is increased to 35 rad/sec in adherence with the design procedure presented in Nissim and Abel (1978). The resulting control laws (A2 and B2) have smaller gains a_T and smaller values of ζ_T as compared with those associated with control laws A1 and B1. Thus, control laws A2 and B2 yield most of their responses in phase with the sensor's velocity over a narrower range of frequencies, with the response peak located much closer to the flutter frequency. These control laws result in sharp increases in the MSV's, accompanied by large increases in the positive phase margins. Therefore, the inboard accelerometer yields MSV = 0.59, with phase margins of $-65°$ and 50° and gain margins of -6.61 and $+\infty$ dB. The outboard accelerometer yields MSV = 0.56, with phase margins of $-68°$ and 45° and gain margins of -7.31 and 10.3 dB. This increase in robustness is consistent with the predictions made by the aerodynamic energy approach. It is achieved at the expense of a considerable increase in the minimum control surface rms rates that reach values of approximately 207 to 211 deg/sec.

To improve the synthesis technique, an attempt was made to incorporate the minimum singular value into the target function J so that

$$J = \dot{\delta}_{\text{rms}} + W_s(\underline{\sigma} - \underline{\sigma}_D)^2 \tag{14}$$

where $\underline{\sigma}$ denotes the MSV over the whole frequency range, and $\underline{\sigma}_D$ denotes the desired value of $\underline{\sigma}$. The factor W_s represents the relative weight given to the MSV in the target function. The optimizer was modified to handle discontinuities. Control laws A3 and B3 were obtained using $W_s = 1000$, $35 \leq \omega_{n_i T} \leq 70$ rad/sec, and $\underline{\sigma}_D = 0.9$ for control law A3 and $\underline{\sigma}_D = 0.8$ for control law B3. The results obtained are shown in figures 12 and 13 and in table 2. The main effect of introducing the MSV into the target functions is to further reduce the gains a_T. Also, although the MSV's increase so that $\underline{\sigma} = 0.65$ for control law A3 and $\underline{\sigma} = 0.64$ for control law B3, the negative gain margins are reduced in magnitude compared with control laws A2 and B2. It is difficult to observe improvements in phase margins in control law A3 when compared with control law A2 even if the sign of the margins is considered unimportant. Yet there is a definite improvement in the value of $\underline{\sigma}$. This point is discussed in more detail later in the report. The values of the MSV's and the values of the phase and gain margins produced by control laws A2, A3, B2, and B3 are very close to those presented in table 1, based on the optimum control theory, and even exceed them in some cases.

The performance of control laws A3 and B3 at dynamic pressures Q below the design dynamic pressure Q_D are tested at $Q = 134$ lb/ft^2 and $Q = 124$ lb/ft^2. The results are summarized in table 2. The decrease in dynamic pressure is accompanied by a slight increase in the MSV's and a significant increase in both phase and gain margins. Thus, discrepancies between the MSV's and the phase and gain margins are again observed. As expected, control surface activity reduces significantly with the decrease in Q.

The performance of control laws A3 and B3 in flutter suppression is shown in the root locus plots in figures 14 and 15. The flutter dynamic pressure is increased from $Q_F = 99$ lb/ft^2 to $Q_F = 175$ lb/ft^2 for control law A3 and to $Q_F = 178$ lb/ft^2 for control law B3.

The previously mentioned small changes in the MSV's as the dynamic pressure was lowered, using control laws A3 and B3, prompted the next examples in this report. This involved the reoptimization of control laws A3 and B3 assuming $Q_D = 124$ lb/ft^2. The results are presented in table 2 as control laws A4 and B4. There is a noticeable increase in the MSV's leading to $\underline{\sigma} = 0.83$ for control law A4 and $\underline{\sigma} = 0.82$ for control law B4. The phase margins are also improved. The smallest improvements are obtained in the negative gain margins. In all cases the control surface activities decrease with Q_D.

Finally, control law B3 was reoptimized by removing the lower bound on $\omega_{n_i T}$, much below $\omega_{n_i T} = 35$ rad/sec, while keeping the target function in the form of equation (13) with $W_s = 1000$. The results obtained were identical to those of control law B3, thus indicating that the constraint is effectively nonactive.

The results presented in table 2 and in figures 12–15 can be summarized by stating that the bounds imposed on $\omega_{n_i T}$ by the aerodynamic energy approach can be substituted by a target function of the form given by equation (13) involving minimum singular values and the rms deflection rates. Control surface activity is always reduced as Q and Q_D both decrease. For a given Q_D, small changes in $\underline{\sigma}$ are observed as Q is reduced. However, large changes in $\underline{\sigma}$ are observed as Q_D is reduced, thus indicating a limit to robustness obtained for any chosen Q_D. This robustness decreases as Q_D increases. If both robustness and Q_D need to be increased, additional or larger control surfaces must be considered. The term robustness is used loosely since improvements in phase and gain margins do not always correlate with improvements in MSV's. However, the target function of the form of equation (13) is adopted for the remainder of this work as a substitute for the constraints imposed on $\omega_{n_i T}$.

In all cases, robustness is increased at the expense of increased control surface activities. This manifests itself in terms of control laws with smaller gains of a_T and smaller values of ζ_T.

Case 2—Control Laws Synthesized With Actuator and With Structural Filter

Definition of the Form of the Required Control Law

The general form of control laws treated thus far can be written as

$$\delta = \frac{4\,a_T}{(s^2 + 2\omega_{n,T}\zeta_T s + \omega_{n,T}^2)} \frac{\ddot{h}_s}{b} \tag{15}$$

where $\ddot{h}_s$ denotes either the outboard or the inboard sensor. The introduction of an actuator and a structural filter clearly affects the control law so that the actual control deflections will no longer have a large inphase component, with the velocity of the driving sensor over a wide range of frequencies spanning the flutter frequency. Also, if sufficient care is not exercised, the control law–actuator combination may lead to control deflections with large components in antiphase, with the velocity of the driving sensor at relatively low frequencies leading to instability of otherwise stable modes.

The basic approach adopted in this report assumes equation (14) to be the desired control deflection–sensor movement relation. The actuator is compensated for as much as possible, with more weight given to the lower frequency range. Following this initial compensation, the resulting control law is optimized in much the same way as in case 1.

Starting first with the structural filter given by equation (6), note that the filter's poles are high enough so that their effects on the low frequencies adjacent to the flutter frequency can be neglected with no need for compensation. The effects of the actuator given by equation (4) can be partly compensated and partly minimized by writing equation (14) in the following form while replacing δ by δ_c:

$$\delta_c = \frac{\gamma_4}{\gamma_1\gamma_3}\frac{(s+\gamma_1)}{(s+\gamma_4)} 4\,a_T \frac{(s^2 + \gamma_2 s + \gamma_3)}{(s^2 + 2\omega_{n,T}\zeta_T s + \omega_{n,T}^2)} \frac{\ddot{h}_s}{b} \tag{16}$$

The final control deflection–sensor movement relation is given by the following expression using equations (4), (6), and (15):

$$\delta = \frac{1.915 \times 10^7}{(s+214)(s^2 + 179.4\,s + 8.945 \times 10^4)} \times \frac{\gamma_4}{\gamma_1\gamma_3}\frac{(s+\gamma_1)}{(s+\gamma_4)} \frac{4\,a_T(s^2 + \gamma_2 s + \gamma_3)}{(s^2 + 2\omega_{n,T}\zeta_T s + \omega_{n,T})} \times \frac{(628)^2}{(s+628)^2}\frac{\ddot{h}_s}{b} \tag{17}$$

Initially, if $\gamma_1 = 214$, $\gamma_2 = 179.4$, $\gamma_3 = 8.945 \times 10^4$, and γ_4 is assigned a high value such as $\gamma_4 = 630$, then the numerators in equation (16) cancel the actuator poles. All that remains is the relation shown in equation (14), together with additional poles that affect only the high-frequency range. These poles could be shifted to even higher values, if necessary. Equation (16) is clearly *dependent on the form of the actuator transfer function.* The design procedure involving the previous control law requires the initial assignment of numerical values to all the constants in equation (17). The γ's are assigned the values stated earlier, with γ_1 slightly reduced to compensate for the phase lags introduced around the flutter frequency by the structural filter and by $(s + \gamma_4)$. The parameters a_T, $\omega_{n,T}$, and ζ_T are initially assigned the values associated with control laws having no actuator, as those obtained in case 1 of this report. Once the system is stabilized at Q_D following the assignment of the previous initial values, the response of the system to gust is used in much the same way as in case 1 to yield optimum values for all γ's, a_T, $\omega_{n,T}$, and ζ_T. More parameters are now available to the designer during the optimization stage, with more freedoms for the system to reach a possibly better optimum.

This manner of introducing the actuator is more consistent with the aerodynamic energy approach than is the Newsom et al. (1980) approach. All phase compensations in Newsom et al. (1980) were made through a single lead

term that restored the phase values only around the flutter frequency. Clearly, at frequencies other than the flutter frequency, such a method yields a control–sensor output relation that is far different from the one warranted by the aerodynamic energy method.

Presentation of Results

Control law A5 uses the inboard accelerometer and control law B5 uses the outboard accelerometer. These control laws were obtained following the design procedure previously described using the parameters associated with control laws A3 and B3 designed in case 1. The resulting optimized control law parameters are presented in appendixes A and B. The results associated with these control laws are presented in figures 16–23 and are summarized in table 3.

In table 3, the MSV's are slightly larger than those obtained for control laws A3 and B3, with $\underline{\sigma} = 0.67$ for both control laws. Similar smaller improvements are also noted in the phase margins (−55° and 59° for control law A5 and −61° and 60° for control law B5). More significant improvements in rms control deflection rates occur, yielding $\dot{\delta}_{rms} = 204.3$ deg/sec for control law A5 and $\dot{\delta}_{rms} = 206.8$ deg/sec for control law B5. The Nyquist plots associated with these two control laws are shown in figures 16 and 17 at the design dynamic pressure $Q_D = 142.6$ lb/ft^2.

Table 3 summarizes the performance of these control laws at dynamic pressure lower than Q_D, and the associated Nyquist plots are presented in figures 18–21. The closed-loop root locus plots are shown in figures 22 and 23. Values for the MSV's remain unchanged as Q is reduced to $Q = 134$ lb/ft^2 and $Q = 124$ lb/ft^2. However, both the phase and gain margins show significant improvement as Q is reduced. Some clarification of requirements is necessary, and a decision must be made as to what is more important—phase and gain margins or minimum singular values. This conflict is discussed in a later section of the report.

Finally, these improvements in robustness of control laws A5 and B5, compared with A3 and B3, are accompanied not only by a decrease in control surface rms activity, but also by an increase in closed-loop flutter dynamic pressure. In figures 22 and 23, the flutter dynamic pressures associated with control laws A5 and B5 are given by $Q_F = 193$ lb/ft^2 and $Q_F = 189$ lb/ft^2, respectively. These values are higher than the values obtained for control laws A3 and B3 designed for the case where no actuator and no structural filter are present. Thus, the introduction of the actuator and filter into the design procedure does not degrade the resulting performance, but noticeably improves it.

Case 3—Results for Systems With Actuator Only, Without Structural Filter

The structural filter was introduced in Newsom et al. (1980) based on engineering judgment only. However, the work in Mukhopadhyay et al. (1981) used the same mathematical model of the DAST–ARW1, but the authors chose not to use a structural filter. Therefore, the work described in case 2 is repeated in case 3, but without the structural filter defined by equation (6).

The results obtained are summarized in table 4 and are presented in part in figures 24 and 25, with control law parameters presented in appendixes A and B. Note that the removal of the structural filter results in both a reduction in control surface activity and in an increase in robustness, both in terms of MSV's and in phase and gain margins. The MSV for control law A6 associated with the inboard accelerometer is $\underline{\sigma} = 0.74$, and for control law B6 the MSV associated with the outboard accelerometer is $\underline{\sigma} = 0.79$. An improvement in phase and gain margins can also be noted, with control law A6 yielding phase margins of −64° and 61°, and with gain margins of −5.01 and 15.39 dB. Control law B6 yields phase margins of −69° and 62°, with gain margins of −5.3 and 14.33 dB. The control surface rms rate for both control laws is approximately 191 to 192 deg/sec. The performance of these two control laws at dynamic pressures below Q_D is summarized in table 4. As Q decreases, the MSV's vary slightly, whereas both the

phase and gain margins improve considerably. Also, in agreement with all previous control laws, control surface activity decreases with Q. The flutter dynamic pressure is increased for both control laws to $Q_F = 206$ lb/ft^2.

Finally, control law B6 was redesigned at a higher Q_D using the outboard accelerometer only. This was done at $Q_D = 151$ lb/ft^2 to compare the results obtained in this report with those reported in Mukhopadhyay et al. (1981) at $Q_D = 160$ lb/ft^2. The ratio between these two values for Q_D is identical to the ratio between the open-loop flutter dynamic pressures obtained in this report and in Mukhopadhyay et al. (1981). The results relate to control law B7, and are summarized in table 4 and presented in figures 24 and 25. Note that despite the previously mentioned increase in Q_D, the MSV and the control surface deflection rate are only slightly reduced.

Minimum Singular Values Compared With Phase and Gain Margins

It is often stated that MSV's lead to conservative estimates regarding bounds of phase and gain margins. Therefore, they should not serve as a means of actual design of robust control laws (too conservative). This investigation involves a single input–single output (SISO) system and is very convenient for the consideration of this issue because Nyquist plots are meaningful for SISO systems and their relation to the MSV's can be readily considered.

Consider the return difference $(1 + GH)$ of a SISO system. The singular value σ of this system at a given frequency is given by the absolute value of the scalar $(1 + GH)$, whereas the Nyquist plot represents the values of the complex scalar GH at the different frequencies. Thus, one can write

$$\sigma = |(GH - (-1))|$$

or

$$\sigma = R$$

where R represents the radius vector joining any point from the Nyquist diagram to the -1 point, as shown in the following sketch. Clearly R is a function of the frequency ω and, therefore, the minimum singular value $\underline{\sigma}$ is equal to the minimum value of R connecting point -1 to the Nyquist curve, as with point C in the sketch. The MSV relates to a point where the *combined* phase and gain variations are closest to the unstable condition.

To demonstrate the problems which may arise with phase and gain margins, consider the following Nyquist diagram. Both the gain and phase margins are very good. However, a small variation in gain can *drastically reduce*

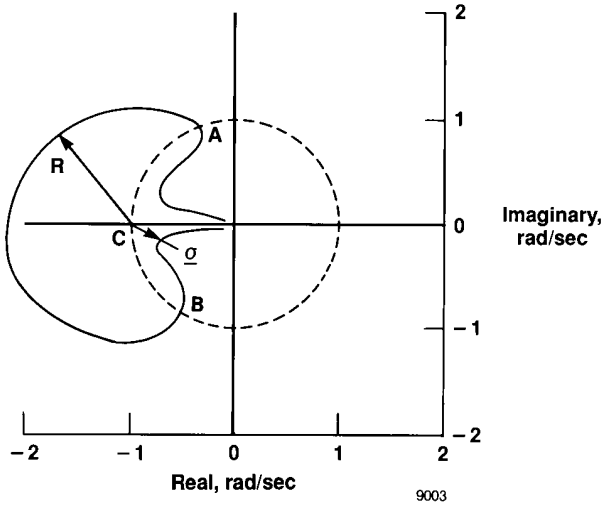

the phase margins. A Nyquist plot of this type is not atypical. An example similar to this sketch is given in figure 19. Other figures in this report can also support the argument. Similarly, small changes in phase margins can lead to large changes in gain margins, as illustrated in the following sketch. Figure 6 shows that this is possible, although in a less extreme form. This illustrates that there is no direct correlation between MSV's and the phase and gain mar-

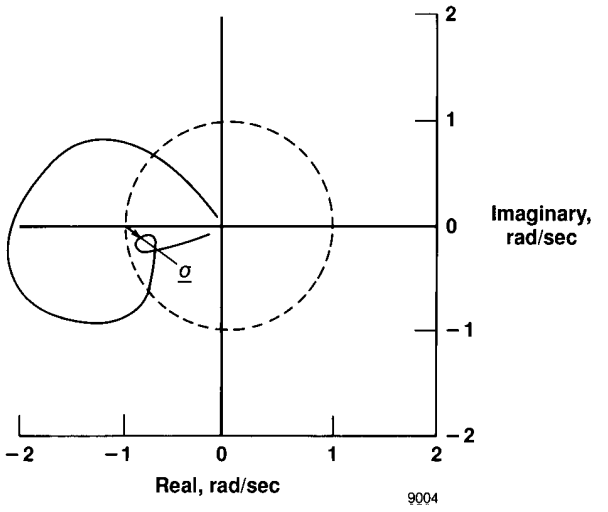

gins. On the basis of the results obtained in this report and the previous discussion, it can be stated that phase and gain margins do *not* present a proper criterion by which robustness can be measured. Future designs should relate to MSV's *only*, and *no* attempts should be made during the design process to associate these values to either phase or gain margins. Therefore, in the remainder of the report robustness will be measured in terms of MSV's only.

Discussion of Results

The results shown in table 2 relating to control laws designed with no actuators indicate that the constraints imposed on the values of $\omega_{n_1 T}$ and $\omega_{n_1 L}$ by the aerodynamic energy approach are necessary to ensure the robustness of the synthesized system. This point explains why the design based on the aerodynamic energy concept in Newsom et al. (1980) yielded relatively low robustness. Newsom et al. (1980) imposed almost no constraints on the values of $\omega_{n_1 T}$. Once the $\omega_{n_1 T}$ constraints are imposed, yielding control laws A2 and B2, the MSV's were fairly close to those obtained while trying to maximize $\underline{\sigma}$, yielding control laws A3 and B3. Also, in the range of values assumed for Q_D, the values of $\underline{\sigma}$ became significantly larger as Q_D was decreased. However, for a given value of Q_D, the value of $\underline{\sigma}$ varied slightly as Q was reduced. This latter effect is shown in all of the tables.

Some interesting results of this report relate to those obtained when actuator dynamics were introduced (see tables 3 and 4). The inclusion of actuator dynamics did not deteriorate the performance, but actually gave better results than those associated with no actuators. Table 3 shows that although the MSV's are only slightly improved when compared with table 2, control surface activity is significantly reduced. Further improvements are also shown in table 4 with the structural filter removed. Again, the improvements encompass both the MSV's and the control surface activities, with all minimum singular values assuming values above $\underline{\sigma} = 0.74$ and with some MSV's reaching as high a value as $\underline{\sigma} = 0.79$. The results presented in tables 3 and 4 exceeded those presented in table 1 that were obtained by various authors based on variations of optimal control theory. Higher order control laws introduce more freedoms through which robustness can be improved, together with reduced control surface activities.

Examine whether the resulting control laws exhibit a large component of control deflection that is in phase with the velocity of the sensor. Plots of δ/h_s as a function of frequency are shown in figures 26–33. For each control law, two plots are presented: one with the imaginary component of δ/h_s that is in phase with the velocityat the sensor's location when it assumes positive values, and one with the real component of δ/h_s. Plots are presented for most of the control laws appearing in tables 1–4, with an additional control law taken from Mukhopadhyay et al. (1981), equation (29). The control law taken from this latter equation was derived using the truncation and reoptimization method, but without the robustness recovery obtained through the introduction of a fictitious noise at the input.

The resulting control law yields poor phase and gain margins. Its δ/h_s plots are shown in figure 28. In the future, control laws with low values of $\underline{\sigma}$ have either smaller positive imaginary values of δ/h_s or else the positive imaginary values span a more limited range of frequencies. This again is in accordance with the results of the aerodynamic energy approach. When δ/h_s has a negative imaginary part (that is, control deflections are in antiphase with the velocity of the driving sensor), the T.E. active control system is likely to have a destabilizing effect. However, if this occurs at sufficiently high frequencies, the neighboring structural modes should be stiff enough and should remain stable. This is true provided the values associated with the negative imaginary parts of δ/h_s are kept reasonably small.

The simplified design procedure, based on the LDTTF with no actuators, yields results only slightly inferior to those obtained using actuators and compensating lead–lag terms. Thus, this simplified design procedure can be used during preliminary design stages, or in conjuction with large packages involving optimization of the structure along with its active control system. Final designs that include actuators can be left to the final stages after the structure assumes its final form.

Finally, this report shows that no distinct relative advantages can be attached to either sensor location. Nonetheless, the inboard location is advantageous. The actuator reacts directly to the motion at the center of the strip where it is located, rather than to the motion of a remote point that bears no relation to the motion of the active strip. Additional work involving other Mach numbers, or additional configurations, are needed to show the relative advantages of the inboard sensor location.

The optimizer used in this report is a variation of Stewart's adaptation of the Davidon, Fletcher, Powell method (Fletcher and Powell, 1963; Stewart, 1967). The variation introduced permits the values of the optimization parameters to be constrained without using penalty functions as described in Nissim and Abel (1978).

Shortly after the introduction of equation (13) as a target function, the optimizer exhibited difficulties in converging. These difficulties were eventually traced to the discontinuous nature associated with the minimum singular values. For purposes of illustration, assume that (1) the term associated with the singular values is the dominant term in equation (13); (2) two singular values have the same minimum value (that is, $\sigma_1 = \sigma_2 = \underline{\sigma}$, as shown in

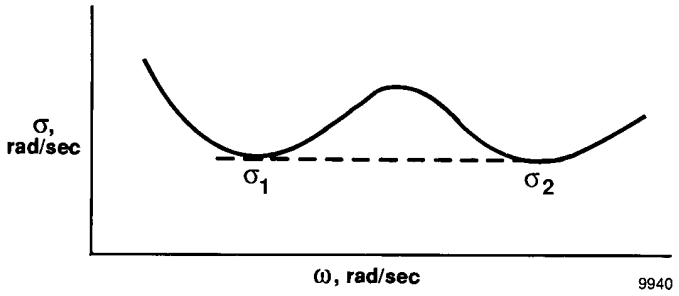

the sketch); and (3) a parameter change that increases any one of these singular values decreases the other one, and conversely. This introduces a discontinuity, making it impossible for the optimizer to make any progress.

To counteract such a situation, the optimizer was modified so that it tested for additional singular values within a chosen small radius from the value of $\underline{\sigma}$ at frequencies that are not immediately adjacent to the frequency associated with $\underline{\sigma}$. When such points were found, the derivatives with respect to the design parameters were evaluated by *both* forward and backward differencing. If the derivatives evaluated by forward differencing were found to change their sign when computed by backward differencing, then those derivatives were assigned the value of zero. Once these modifications were introduced, no convergence problems were encountered.

Summary of Proposed Control Law Synthesis Technique

The following control law synthesis procedure is suggested based on the foregoing discussion. However, variations to this procedure can be made once sufficient experience is gained using this method.

1. Choose the localized damping-type transfer function with no actuators.
2. Choose initial values for a_T, $\omega_{n,T}$, and ζ_T (or a_L, $\omega_{n,L}$, and ζ_L) for all active control surfaces to stabilize the system at Q_D and at the highest subsonic Mach number.
3. Optimize for the design parameters that minimize control surface activity, putting no active constraints on the values of ω_n.

4. Introduce the minimum singular values into the target function (eq. (13)) and reoptimize the design variables, with initial values set to the optimal values obtained in step 2.

5. Repeat step 4, if necessary, using different values for W_s and $\underline{\sigma}_D$ until either a desired value for $\underline{\sigma}$ is obtained, or until $\underline{\sigma}$ reaches an asymptotic value.

6. Introduce the actuator and use as initial values (for the design parameters) the values associated with the optimized control law obtained in step 5, together with the actuator compensation terms, as shown earlier. Reoptimize to obtain the final optimum values for the design parameters.

7. Test the performance of the resulting control law over a range of Mach number and flight configurations.

This procedure not only yields the required control law, but it also provides the designer with physical insight regarding the system. Step 2, for example, can be skipped, although it provides the designer with the minimum value of control surface activity irrespective of robustness requirements. This is useful since, as already shown, robustness is achieved at the cost of increased control surface activity. Steps 3–6 can also be skipped. Step 3 can be replaced with a constrained optimization, with ω_n limited between 0.65 ω_F and 1.45 ω_F if this method is to be used in a preliminary design stage in conjunction with a large structural–aeroservoelasticity optimization package. Steps 3–6 can be left to the final design stage in this latter case.

Finally, in many instances the optimizer went to the absolute minimum of control surface activity associated with zero gains; that is, $a_L = a_T = 0$. This was easily avoided by imposing a lower bound on the gains. In this report, $a_T \geq 0.5$ yields satisfactory results, with the lower bound never turning to produce an active constraint.

CONCLUDING REMARKS

The aerodynamic energy approach yields low-order control laws with performances superior to those obtained using optimal control theory-based synthesis methods. Unlike previous works associated with the aerodynamic energy method, there is no single specific control law, but instead an infinite number of control laws that result from the aerodynamic energy method. Also, higher order control laws, while still maintaining relatively low orders, provide the system with more freedom to reduce control surface activities with a desired level of robustness. With sensors positioned around the locations required by the aerodynamic energy approach, *all* robust control laws, irrespective of the method of synthesis, yield a large component of trailing-edge control rotation in phase with the velocity of its driving sensor. This is true over a wide range of frequencies that span the flutter frequency. The latter result is in accordance with the damping-type transfer function results obtained while developing the aerodynamic energy approach.

A redefined synthesis procedure is suggested that replaces previous constraints imposed by the aerodynamic energy approach, with a target function that includes minimum singular values. The redefined procedure gives some weight to robustness while optimizing the design parameters. This is important since it is shown that robustness is achieved at a cost of increased control surface activity.

It is hoped that additional examples relating to specific mathematical models will reconfirm the superiority of the aerodynamic energy approach regarding the synthesis of low-order control laws for flutter suppression.

APPENDIX A
SUMMARY OF CONTROL LAWS USING THE INBOARD SENSOR

Control Laws for System With No Actuator

Control Law A1, optimized at Q_D = 142.6 lb/ft^2, $\omega_n \geq 2$, $W_s = 0$

$$\frac{\delta}{\frac{h_{inb}}{b}} = \frac{4 \times 2.1 s^2}{s^2 + (2 \times 2 \times 0.90)s + (2)^2} \tag{A-1}$$

Control Law A2, optimized at Q_D = 142.6 lb/ft^2, $\omega_n \geq 35$, $W_s = 0$

$$\frac{\delta}{\frac{h_{inb}}{b}} = \frac{4 \times 1.2 s^2}{s^2 + (2 \times 35 \times 0.29)s + (35)^2} \tag{A-2}$$

Control Law A3, optimized at Q_D = 142.6 lb/ft^2, $\omega_n \geq 35$, W_s = 1000

$$\frac{\delta}{\frac{h_{inb}}{b}} = \frac{4 \times 1.03 s^2}{s^2 + (2 \times 35 \times 0.34)s + (35)^2} \tag{A-3}$$

Control Law A4, optimized at Q_D = 124 lb/ft^2, $\omega_n \geq 35$, W_s = 1000

$$\frac{\delta}{\frac{h_{inb}}{b}} = \frac{4 \times 1.23 s^2}{s^2 + (2 \times 39.3 \times 1)s + (39.3)^2} \tag{A-4}$$

Control Law for System With Actuator and With Structural Filter

Control Law A5, optimized at Q_D = 142.6 lb/ft^2, W_s = 1000

$$\frac{\delta_c}{\frac{\ddot{h}_{inb}}{b}} = \frac{4 \times 1 \times 630}{91.8 \times 52{,}353} \frac{(s + 91.8)(s^2 + 270.9s + 52{,}353)}{(s + 630)[s^2 + (2 \times 25.2 \times 0.29)s + (25.2)^2]} \tag{A-5}$$

Control Law for System With Actuator But With No Structural Filter

Control Law A6, optimized at Q_D = 142.6 lb/ft^2, W_s = 1000

$$\frac{\delta_c}{\frac{\ddot{h}_{inb}}{b}} = \frac{4 \times 1.29 \times 630}{186.6 \times 31{,}494} \frac{(s + 186.6)}{(s + 630)} \frac{(s^2 + 153.6s + 31{,}494)}{[s^2 + (2 \times 15.8 \times 0.39)s + (15.8)^2]} \tag{A-6}$$

APPENDIX B
SUMMARY OF CONTROL LAWS USING THE OUTBOARD SENSOR

Control Laws for System With No Actuator

Control Law B1, optimized at $Q_D = 142.6$ lb/ft^2, $\omega_n \geq 2$, $W_s = 0$

$$\frac{\delta}{\frac{h_{outb}}{b}} = \frac{4 \times 1.72 s^2}{s^2 + (2 \times 2 \times 0.89)s + (2)^2} \tag{B-1}$$

Control Law B2, optimized at $Q_D = 142.6$ lb/ft^2, $\omega_n \geq 35$, $W_s = 0$

$$\frac{\delta}{\frac{h_{outb}}{b}} = \frac{4 \times 0.96 s^2}{s^2 + (2 \times 35 \times 0.31)s + (35)^2} \tag{B-2}$$

Control Law B3, optimized at $Q_D = 142.6$ lb/ft^2, $\omega_n \geq 35$, $W_s = 1000$

$$\frac{\delta}{\frac{h_{outb}}{b}} = \frac{4 \times 0.69 s^2}{s^2 + (2 \times 35 \times 0.31)s + (35)^2} \tag{B-3}$$

Control Law B4, optimized at $Q_D = 124$ lb/ft^2, $\omega_n \geq 35$, $W_s = 1000$

$$\frac{\delta}{\frac{h_{outb}}{b}} = \frac{4 \times 0.72 s^2}{s^2 + (2 \times 35 \times 0.98)s + (35)^2} \tag{B-4}$$

Control Law for System With Actuator and With Structural Filter

Control Law B5, optimized at $Q_D = 142.6$ lb/ft^2, $W_s = 1000$

$$\frac{\delta_c}{\frac{\ddot{h}_{outb}}{b}} = \frac{4 \times 0.7 \times 630}{126.6 \times 42{,}602} \frac{(s + 126.6)}{(s + 630)} \frac{(s^2 + 251.8s + 42{,}602)}{[s^2 + (2 \times 28.7 \times 0.26)s + (28.7)^2]} \tag{B-5}$$

Control Laws for System With Actuator But With No Structural Filter

Control Law B6, optimized at $Q_D = 142.6$ lb/ft^2, $W_s = 1000$

$$\frac{\delta_c}{\frac{\ddot{h}_{outb}}{b}} = \frac{4 \times 0.96 \times 630}{185.8 \times 29{,}658} \frac{(s + 185.8)}{(s + 630)} \frac{(s^2 + 155s + 29{,}658)}{[s^2 + (2 \times 16.5 \times 0.41)s + (16.5)^2]} \tag{B-6}$$

Control Law B7, optimized at Q_D = 151 lb/ft^2, W_s = 1000

$$\frac{\delta_c}{\frac{\ddot{h}_{outb}}{b}} = \frac{4 \times 1.06 \times 630}{189.3 \times 30{,}000} \frac{(s + 189.3)}{(s + 630)} \frac{(s^2 + 156.6s + 30{,}000)}{[s^2 + (2 \times 15 \times 0.37)s + (15)^2]} \tag{B-7}$$

REFERENCES

Doyle, J.C., and G. Stein, "Robustness With Observers," *IEEE Trans. Autom. Control*, vol. AC-24, no. 4, Aug. 1979.

Fletcher, R., and M.J.D. Powell, "A Rapidly Convergent Descent Method for Minimization," *Comput. J.*, vol. 6, no. 2, July 1963, pp. 163–168.

Gangsaas, D. and L. Uy-Loi, "Application of a Modified Linear Quadratic Gaussian Design to Active Control of a Transport Airplane," AIAA-79-1746, Aug. 1979.

Mahesh, J.K., W.L. Garrard, C.R. Stone, and P.D. Hausman, *Active Flutter Control for Flexible Vehicles. Vol. 1—Final Report*, NASA CR-159160, 1979.

Mahesh, J.K., C.R. Stone, W.L. Garrard, and H.J. Dunn, "Control Law Synthesis for Flutter Suppression Using Linear Quadratic Gaussian Theory," *J. Guidance and Control*, vol. 4, no. 4, July–Aug. 1981, pp. 415–422.

Mukhopadhyay, V., "Stability Robustness Improvement Using Constrained Optimization Techniques," *J. Guidance and Control*, vol. 10, no. 2, Mar.–Apr. 1987.

Mukhopadhyay, V., and J.R. Newsom, "Application of Matrix Singular Value Properties for Evaluating Gain and Phase Margins of Multiloop Systems," AIAA-82-1574, 1982.

Mukhopadhyay, V., J.R. Newsom, and I. Abel, *A Method for Obtaining Reduced-Order Control Laws for High-Order Systems Using Optimization Techniques*, NASA TP-1876, 1981.

Mukhopadhyay, V., J.R. Newsom, and I. Abel, "Reduced-Order Optimal Feedback Control Law Synthesis for Flutter Suppression," *J. Guidance and Control*, vol. 5, no. 4, July–Aug. 1982.

Newsom, J.R., I. Abel, and H.J. Dunn, *Application of Two Design Methods for Active Flutter Suppression and Wind-Tunnel Test Results*, NASA TP-1653, 1980.

Newsom, J.R., A.S. Pototzky, and I. Abel, "Design of the Flutter Suppression System for DAST ARW-1R—A Status Report," AIAA-83-0990, 1983.

Newsom, J.R., *A Method for Obtaining Practical Flutter-Suppression Control Laws Using Results of Optimal Control Theory*, NASA TP-1471, 1979.

Nissim, E., "Comparative Study Between Two Different Active Flutter Suppression Systems," *J. of Aircraft*, vol. 15, no. 12, 1978, pp. 843–848.

Nissim, E., *Flutter Suppression Using Active Controls Based on the Concept of Aerodynamic Energy*, NASA TN D-6199, 1971.

Nissim, E., *Recent Advances in Aerodynamic Energy Concept for Flutter Suppression and Gust Alleviation Using Active Controls*, NASA TN D-8519, 1977.

Nissim, E., and I. Abel, *Development and Application of an Optimization Procedure for Flutter Suppression Using the Aerodynamic Energy Concept*, NASA TP-1137, 1978.

Nissim, E., A. Caspi, and I. Lottati, *Application of the Aerodynamic Energy Concept to Flutter Suppression and Gust Alleviation by Use of Active Controls*, NASA TN D-8212, 1976.

Nissim, E., and I. Lottati, "Active Controls for Flutter Suppression and Gust Alleviation in Supersonic Aircraft," *J. Guidance and Control*, vol. 3, no. 4, July–Aug. 1980, pp. 345–351.

Stewart, G.W., III, "A Modification of Davidon's Minimization Method to Accept Difference Approximations of Derivatives," *J. Assoc. Comput. Mach.*, vol. 14, no. 1, Jan. 1967, pp. 72–82.

Table 1. Comparisons between existing and reconstructed results for the DAST–ARW1 mathematical model.

	Q_F, lb/ft^2	ω_F, rad/sec	δ_{RMS}, deg	$\dot{\delta}_{RMS}$, deg/sec	Gain margin, dB		Phase margin, deg		MSV
Open-loop flutter*	99	50	---	---	---	---	---	---	---
	(105)	(51.6)	---	---	---	---	---	---	---
Closed loop with control law given by equation (9)*	174.3	49	---	---	---	---	---	---	---
	(188.5)	(44)	---	---	---	---	---	---	---
Equation (9)*, Q_D = 142.6 lb/ft^2	---	---	3.8	208.9	−5.34	14.29	−48	47	0.606
Equation (9)*, Q_D = 151 lb/ft^2	---	---	(4.1)	(218)	(−6)	(16.5)	(−52)	(52)	(0.64†)
Equation (30)‡	180	39							
	(185)	(36)							
Equation (30)‡, Q_D = 151 lb/ft^2			4.12	213.2	−4.2	13.6	−57	55	0.611
Equation (30)‡, Q_D = 160 lb/ft^2	---	---	(NA)	(NA)	(−5.4)	(12)	(−62)	(57)	0.68†

*Relates to reference 17.

†Values extracted from Nyquist plots.

‡Relates to reference 7.

(Values in parentheses are those obtained from the references.)

Table 2. Summary of results associated with synthesized aerodynamic energy control laws for a mathematical model with no actuators.

Control law	Q_F, lb/ft^2	ω_F, rad/sec	δ_{RMS}, deg	$\dot{\delta}_{RMS}$, deg/sec	Gain margin, dB		Phase margin, deg		MSV	Remarks
A1	---	---	4.35	174.2	−9.34	∞	−112	24	0.353	Optimized at Q_D = 142.6 lb/ft^2,
B1	---	---	4.40	174.7	−10.50	5.19	−130	20	0.313	$\omega_n \geq 2, W_\delta = 0$.
A2	---	---	4.31	211	−6.61	∞	−65	50	0.589	Optimized at Q_D = 142.6 lb/ft^2,
B2	---	---	4.23	207.4	−7.31	10.3	−68	45	0.561	$\omega_n \geq 35, W_\delta = 0$.
A3	175	46.4	4.15	218.5	−4.76	∞	−49	59	0.647	Optimized at Q_D = 142.6 lb/ft^2,
B3	178	45.7	4.05	217	−4.52	13.15	−55	59	0.639	$\omega_n \geq 35, W_\delta = 1000$.
A3, Q = 134 lb/ft^2	---	---	3.56	190.9	6.19	∞	−80	74	0.667	Nyquist plots of control laws at Q =
B3, Q = 134 lb/ft^2	---	---	3.55	193	−5.85	13.64	−86	74	0.657	134 lb/ft^2 optimized at Q_D = 142.6 lb/ft^2.
A3, Q = 124 lb/ft^2	---	---	3	162.3	−9.46	∞	−86	66	0.69	Nyquist plots of control laws at Q =
B3, Q = 124 lb/ft^2	---	---	3.03	166.2	−8.88	14.2	−82	63	0.678	124 lb/ft^2 optimized at Q_D = 142.6 lb/ft^2.
A4	---	---	2.66	147.5	−5.98	∞	−58	80	0.834	Optimized at Q_D = 124 lb/ft^2,
B4	---	---	2.67	150.2	−5.2	30.8	−63	67	0.82	$\omega_n \geq 35, W_\delta = 1000$.

Table 3. Summary of results associated with synthesized aerodynamic energy control laws for a mathematical model with actuator and with structural filter.

Control law	Q_F, lb/ft^2	ω_F, rad/sec	δ_{RMS}, deg	$\dot{\delta}_{RMS}$, deg/sec	Gain margin, dB		Phase margin, deg		MSV	Remarks
A5	193	38.1	4.05	204.3	−4.86	9.63	−55	59	0.669	Optimized at Q_D = 142.6 lb/ft^2,
B5	189	38	4.01	206.8	−4.66	15.09	−61	60	0.669	W_δ = 1000.
A5, Q = 134 lb/ft^2	---	---	3.6	185.2	−6.15	9.63	−90	66	0.675	Nyquist plots of control laws at Q =
B5, Q = 134 lb/ft^2	---	---	3.61	189.9	−5.8	15.65	−98	68	0.668	134 lb/ft^2 optimized at Q = 142.6 lb/ft^2.
A5, Q = 124 lb/ft^2	---	---	3.12	162.1	−9.04	9.92	−119	63	0.682	Nyquist plots of control laws at Q =
B5, Q = 124 lb/ft^2	---	---	3.16	168.1	−8.5	16.31	−77	64	0.659	124 lb/ft^2 optimized at Q = 142.6 lb/ft^2.

Table 4. Summary of results associated with synthesized aerodynamic energy control laws for a mathematical model with actuator but without structural filter.

Control law	Q_F, lb/ft^2	ω_F, rad/sec	δ_{RMS}, deg	$\dot{\delta}_{RMS}$, deg/sec	Gain margin, dB		Phase margin, deg		MSV	Remarks
A6	206	28.2	3.93	192.3	−5.01	15.39	−64	61	0.742	Optimized at Q_D = 142.6 lb/ft^2,
B6	206	29.6	3.87	191.3	−5.3	14.33	−69	62	0.788	W_δ = 1000.
A6, Q = 134 lb/ft^2	---	---	3.63	182.6	−5.93	15.65	−99	72	0.748	Nyquist plots of control laws at Q =
B6, Q = 134 lb/ft^2	---	---	3.57	181.1	−6.32	14.85	−105	69	0.791	134 lb/ft^2 optimized at Q_D = 142.6 lb/ft^2.
A6, Q = 124 lb/ft^2	---	---	3.27	167.2	−8.13	15.65	−134	60	0.756	Nyquist plots of control laws at Q =
B6, Q = 124 lb/ft^2	---	---	3.21	165.5	−8.94	15.49	−134	69	0.771	124 lb/ft^2 optimized at Q_D = 142.6 lb/ft^2.
B7	204	25.4	4.34	189.4	−5.8	13.23	−58	54	0.757	Optimized at Q_D = 151 lb/ft^2.

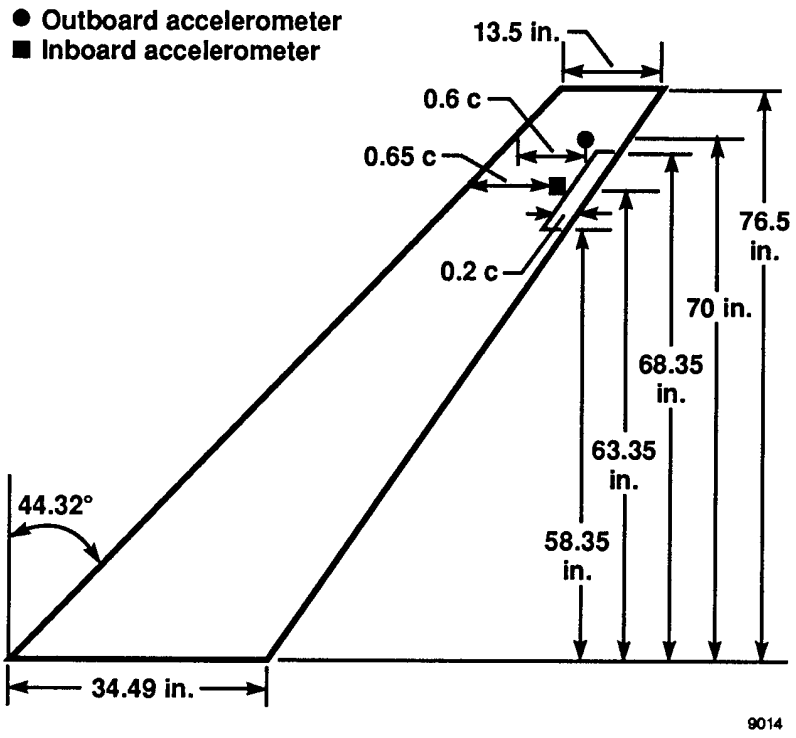

Figure 1. Model geometry.

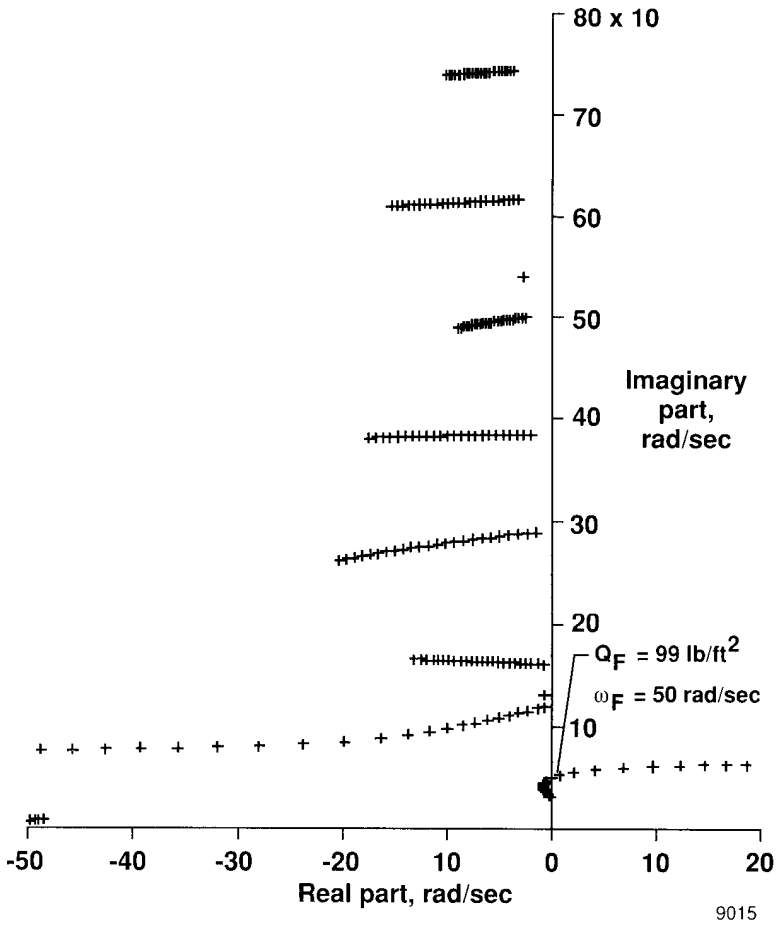

Figure 2. Open-loop root locus plot at $M = 0.9$.

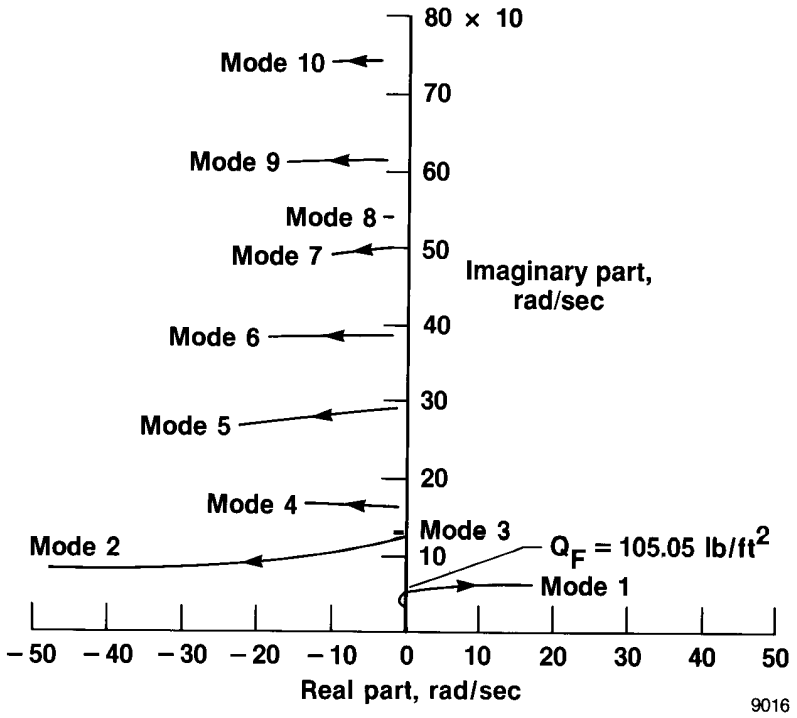

Figure 3. Root locus plot at $M = 0.9$; system off, arrows indicate increasing dynamic pressure. Reproduced from Newsom et al. (1980).

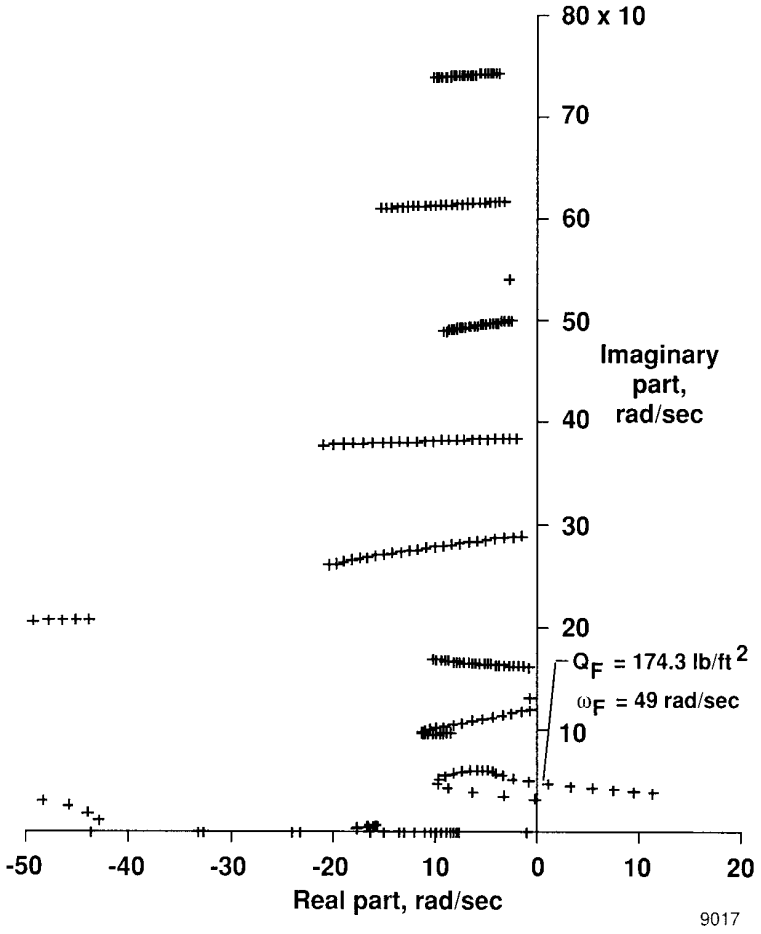

Figure 4. Closed-loop root locus plot using control law given by equation (9), Newsom et al. (1980).

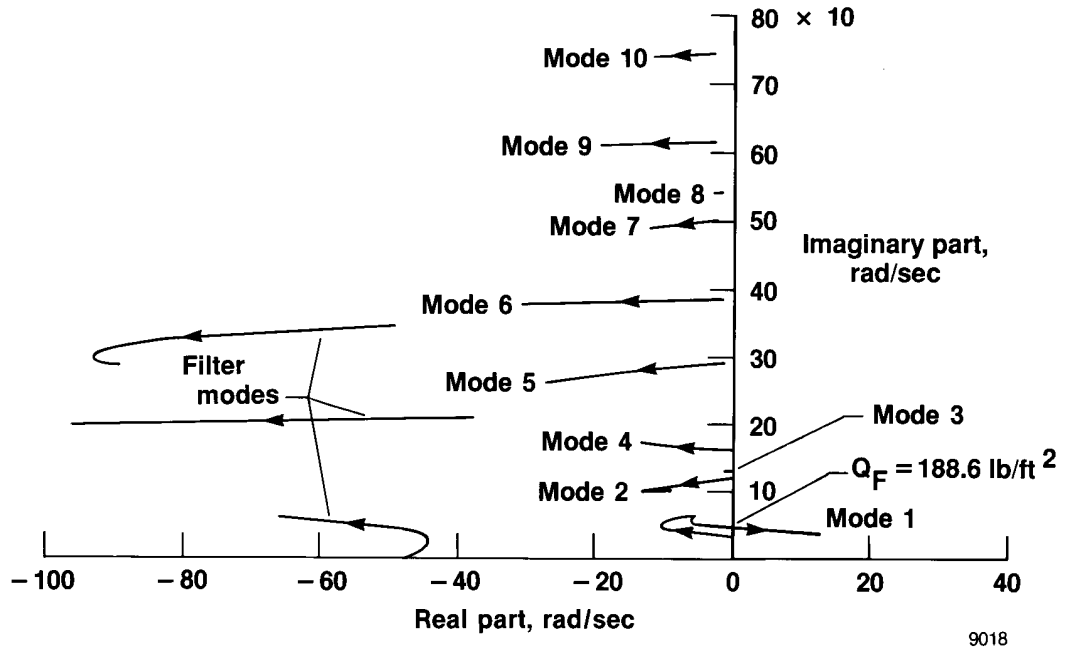

Figure 5. Closed-loop root locus plot at $M = 0.9$; control law defined by equation (9), arrows indicate increasing dynamic pressure. Reproduced from Newsom et al. (1980).

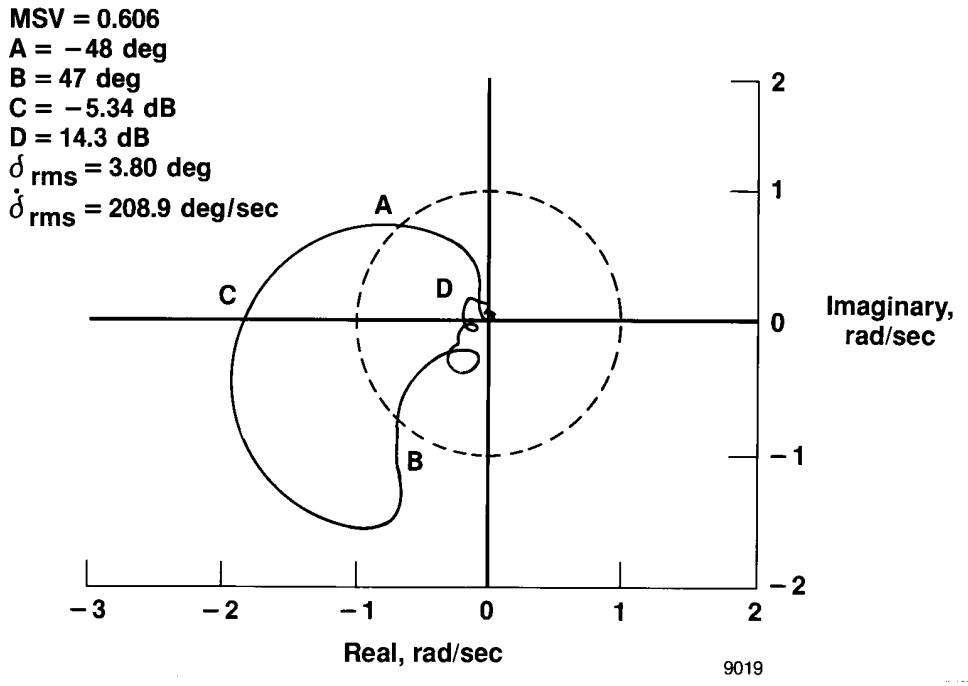

Figure 6. Nyquist plot at $Q_D = 142.6$ lb/ft^2 using control law given by equation (3), Newsom et al.

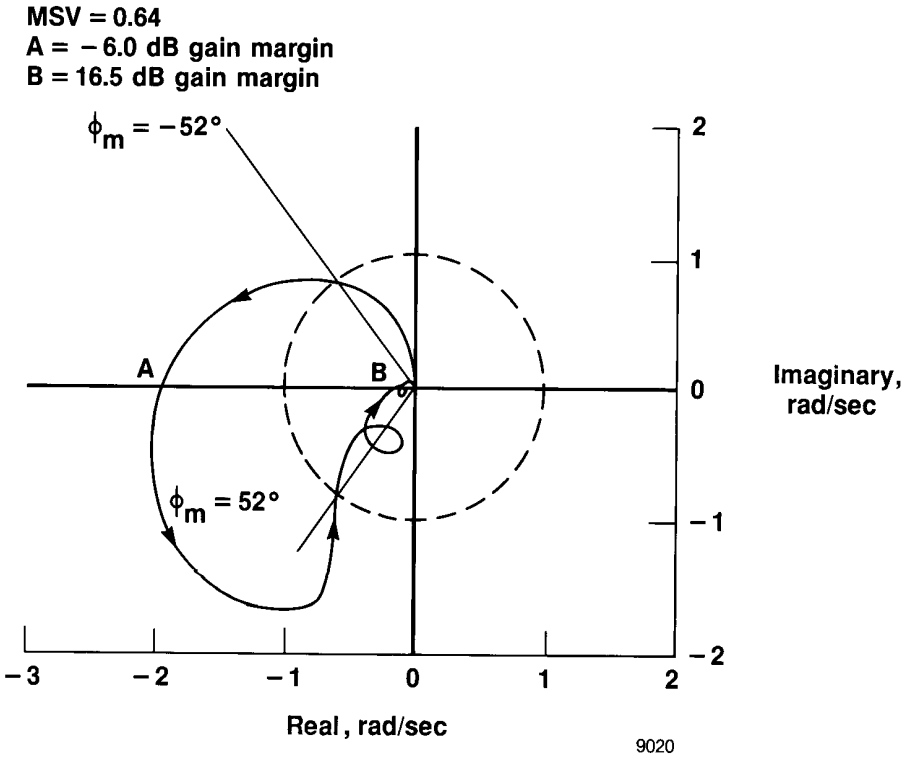

Figure 7. Nyquist plot of open-loop transfer function $G(i\omega)H(i\omega)$; $M = 0.9$, $Q = Q_{max}$; $H(i\omega)$ defined by equation (9), arrows indicate increasing frequency. Reproduced from Newsom et al. (1980).

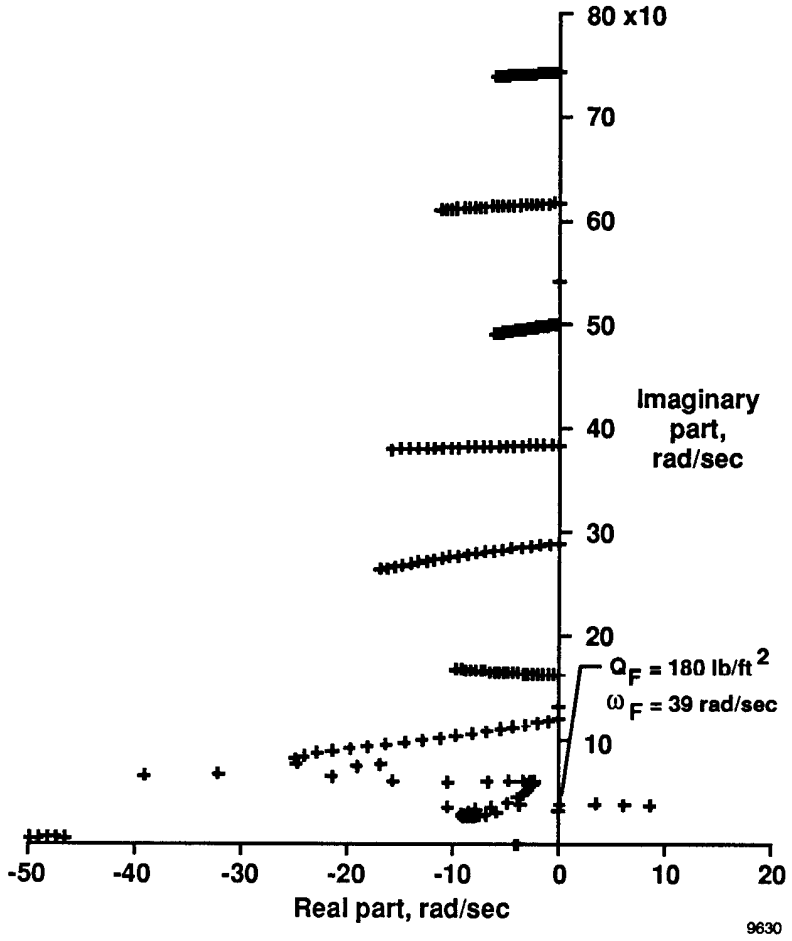

Figure 8. Closed-loop root locus plot using control law given by equation (30), Mukhopadhyay et al. (1981).

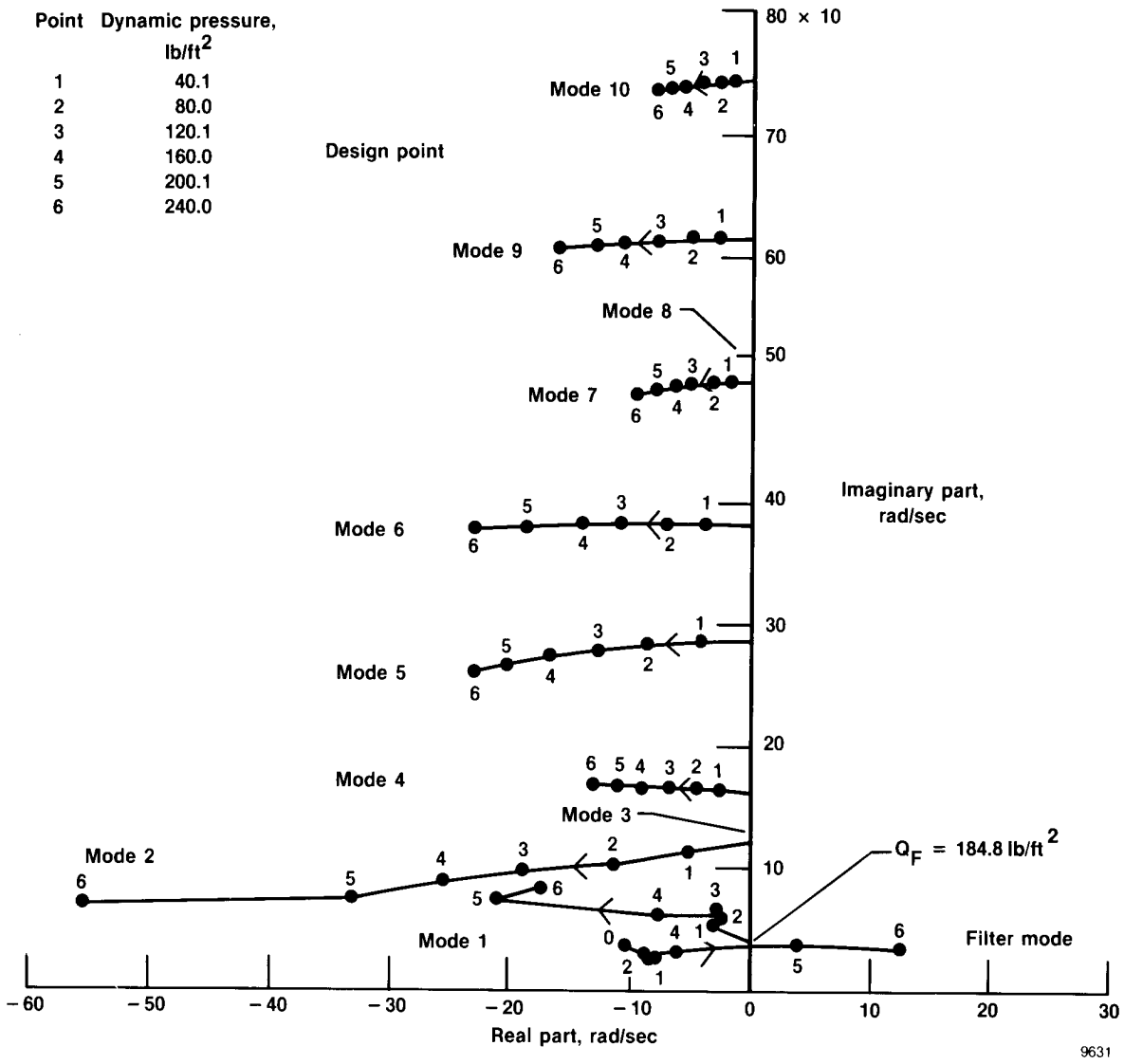

Figure 9. Closed-loop dynamic pressure root locus plot of 65th-order plant plus 4th-order control law. Designed with 25th-order plant, $R_u = 0.00001$. Reproduced from Mukhopadhyay et al. (1981).

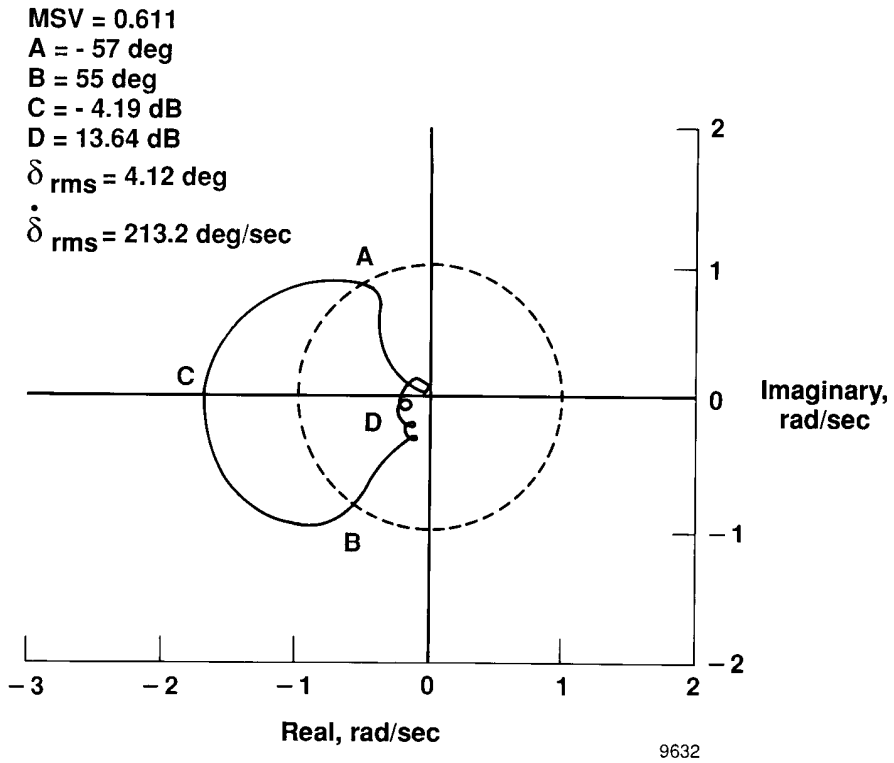

Figure 10. Nyquist plot at Q_D = 151 lb/ft^2 using control law given by equation (30), Mukhopadhyay et al. (1981).

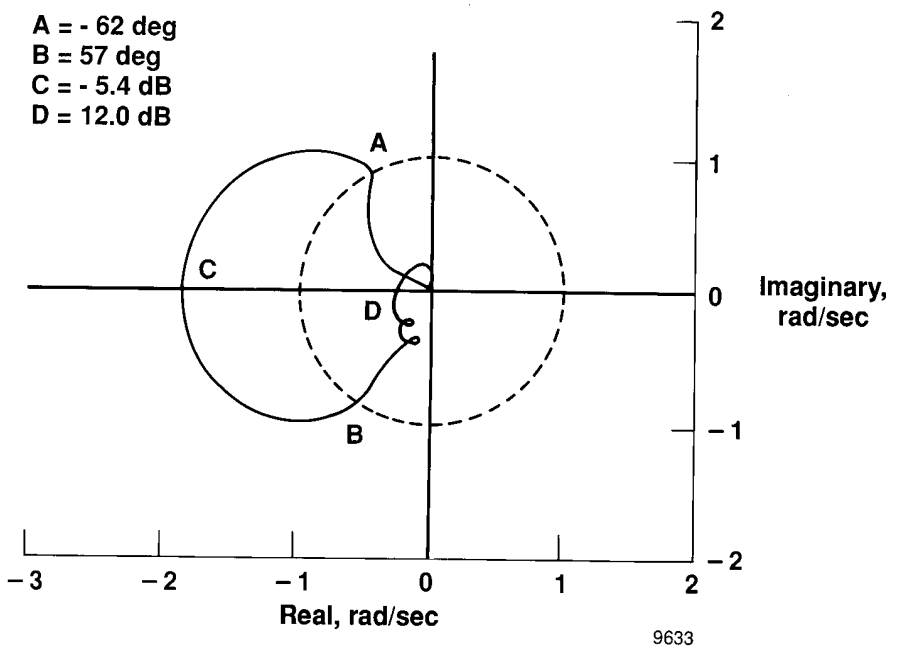

Figure 11. Nyquist plot of 65th-order plant model plus 4th-order control law. Designed with 25th-order plant model, Q = 160 lb/ft^2 and R_u = 0.00001. Reproduced from Mukhopadhyay et al. (1981).

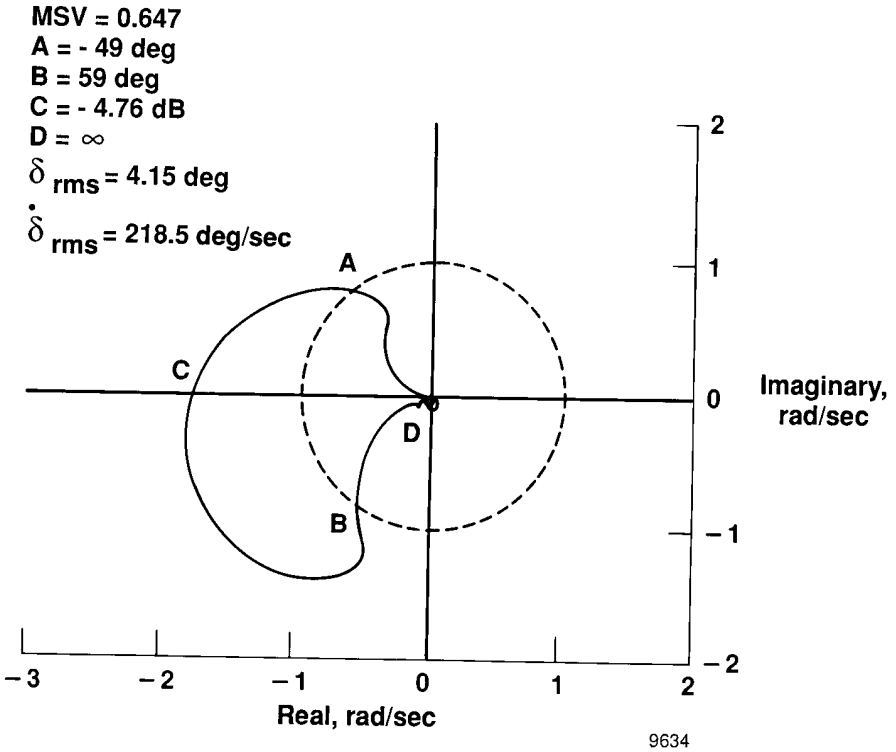

Figure 12. Nyquist plot at Q_D = 142.6 lb/ft^2 using aerodynamic energy control law A3. Optimized with $\omega_{n_T} \geq 35$ rad/sec, W_s = 1000, and ζ_D = 0.8 using inboard accelerometer.

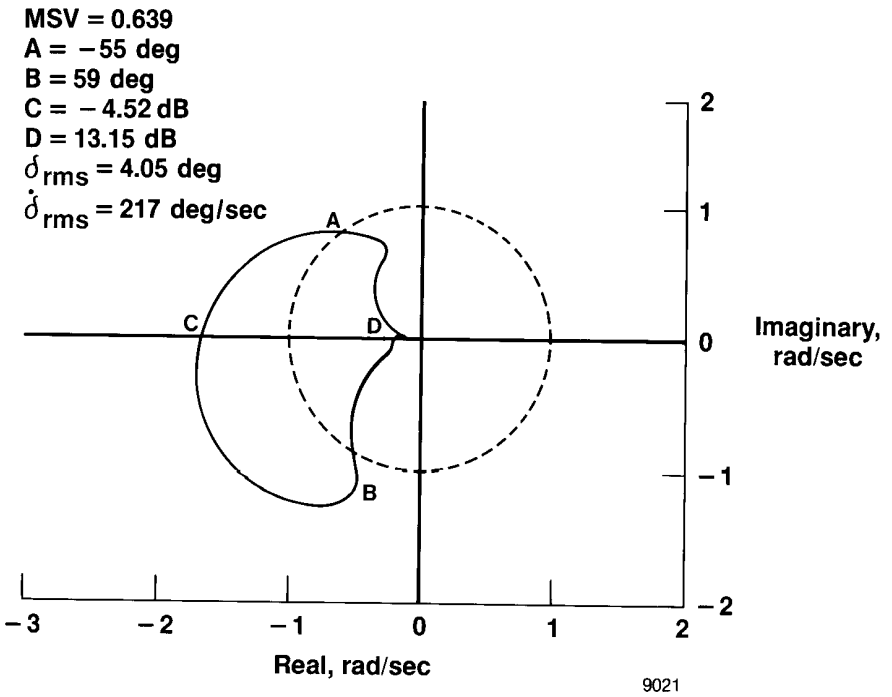

Figure 13. Nyquist plot at Q_D = 142.6 lb/ft^2 using aerodynamic energy control law B3. Optimized with $\omega_{n_T} \geq 35$ rad/sec, W_s = 1000, and ζ_D = 0.8 using outboard accelerometer.

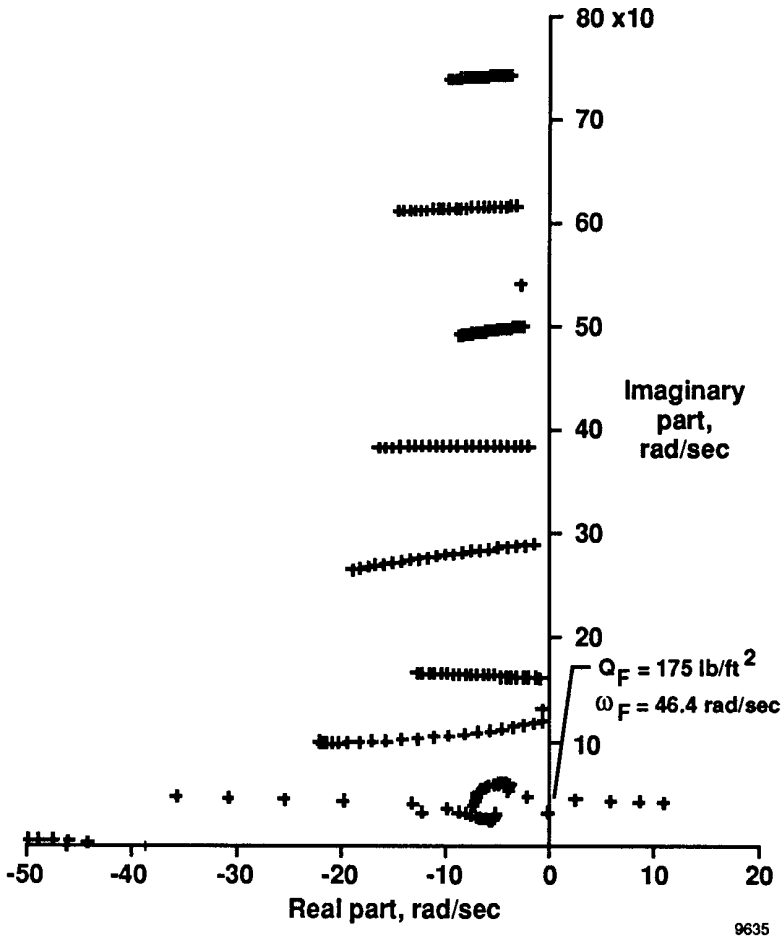

Figure 14. Root locus plot using aerodynamic energy control law A3. Optimized at Q_D = 142.6 lb/ft^2, with W_s = 1000, ς_D = 0.8, and $\omega_{n,T} \geq 35$ using inboard accelerometer.

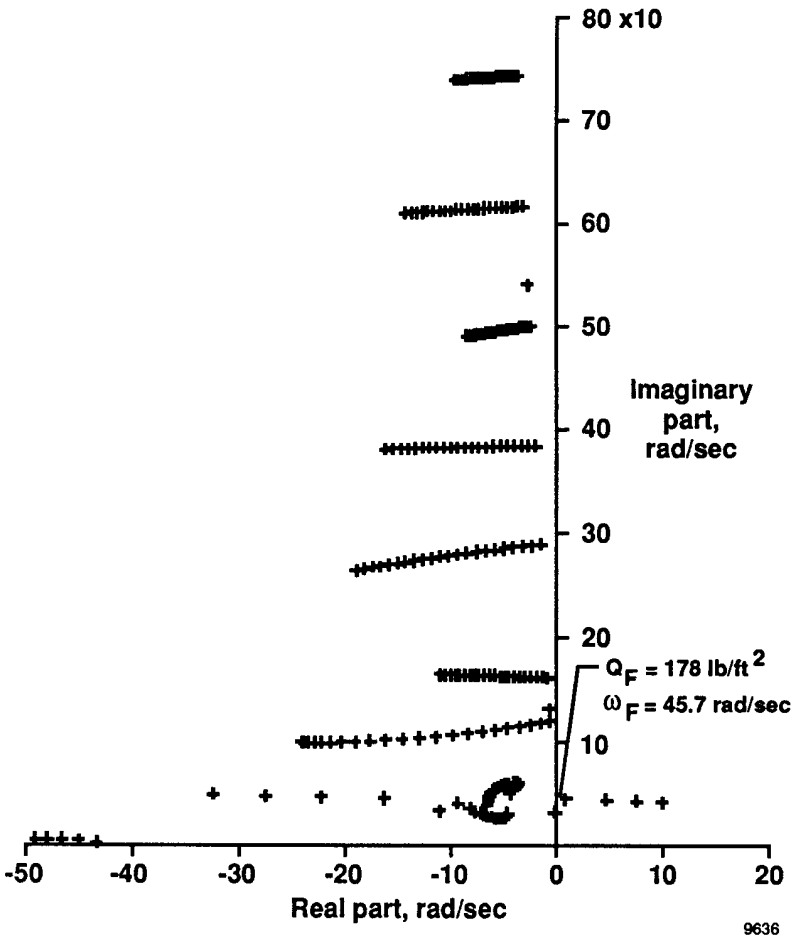

Figure 15. Root locus plot using aerodynamic energy control law B3. Optimized at Q_D = 142.6 lb/ft^2, with W_s = 1000, ζ_D = 0.8, and $\omega_{n_T} \geq 35$ using outboard accelerometer.

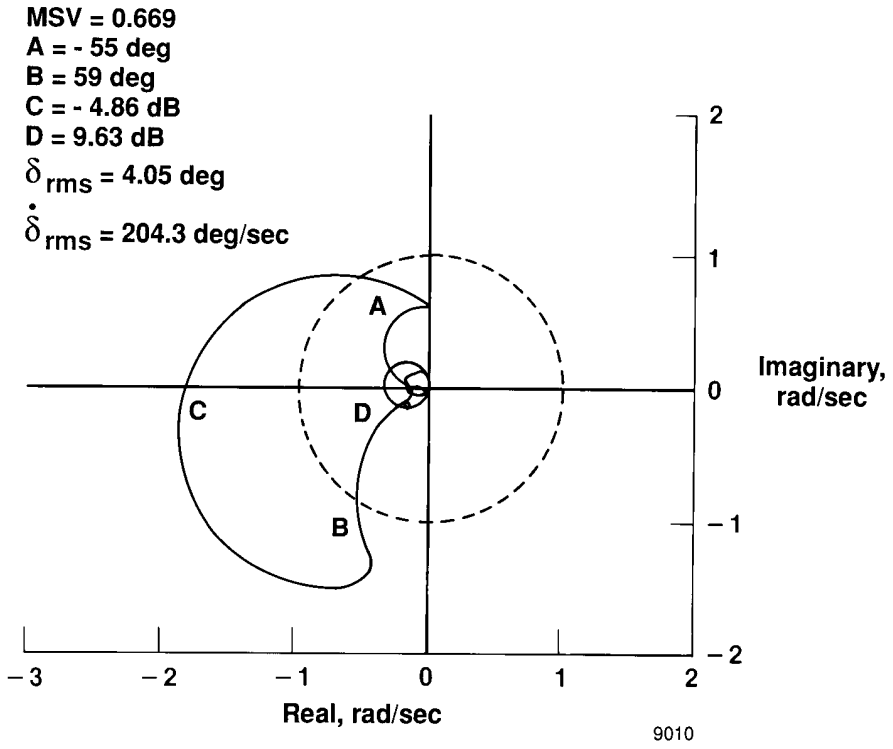

Figure 16. Nyquist plot at Q_D = 142.6 lb/ft^2 using aerodynamic energy control law A5. Optimized with actuator and structural filter at Q_D = 142.6 lb/ft^2, with W_s = 1000, ζ_D = 0.9, and $\omega_{n,T} \geq 25$ using inboard accelerometer.

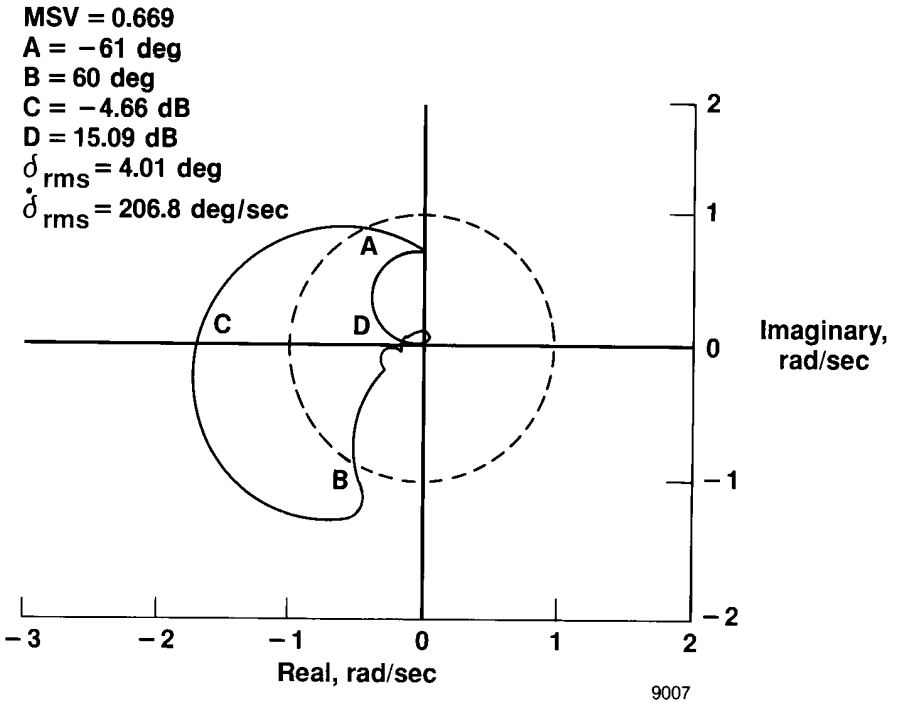

Figure 17. Nyquist plot at Q_D = 142.6 lb/ft^2 using aerodynamic energy control law B5. Optimized with actuator and with structural filter at Q_D = 142.6 lb/ft^2, with W_s = 0, ζ_D = 0.85 using outboard accelerometer.

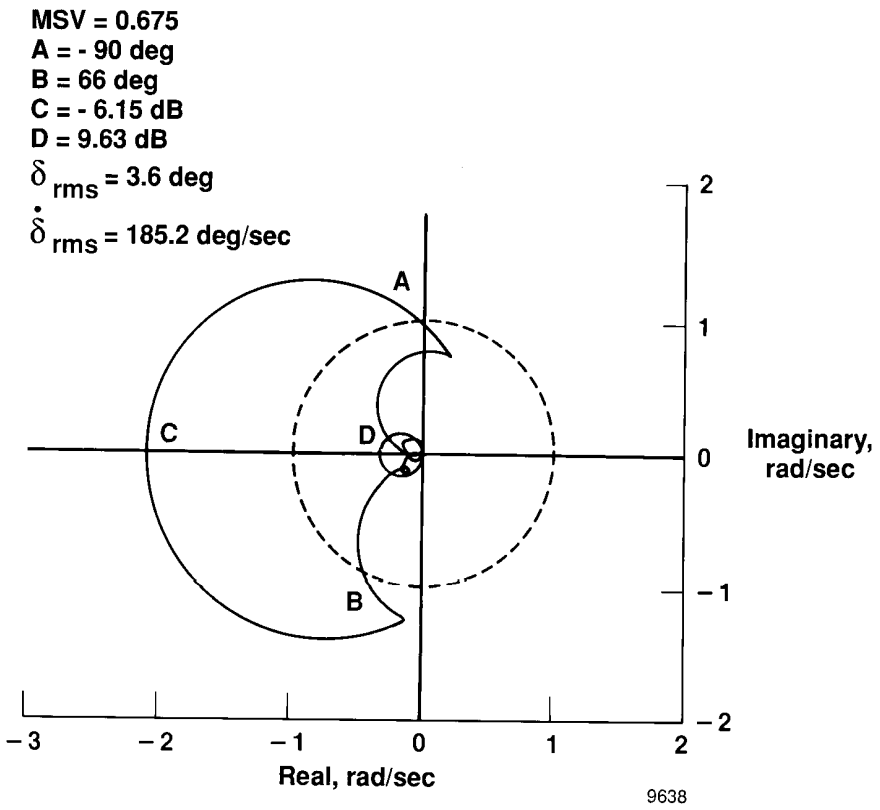

Figure 18. Nyquist plot at Q = 134 lb/ft^2 of aerodynamic energy control law A5. Optimized at Q_D = 142.6 lb/ft^2, with actuator and structural filter using inboard accelerometer.

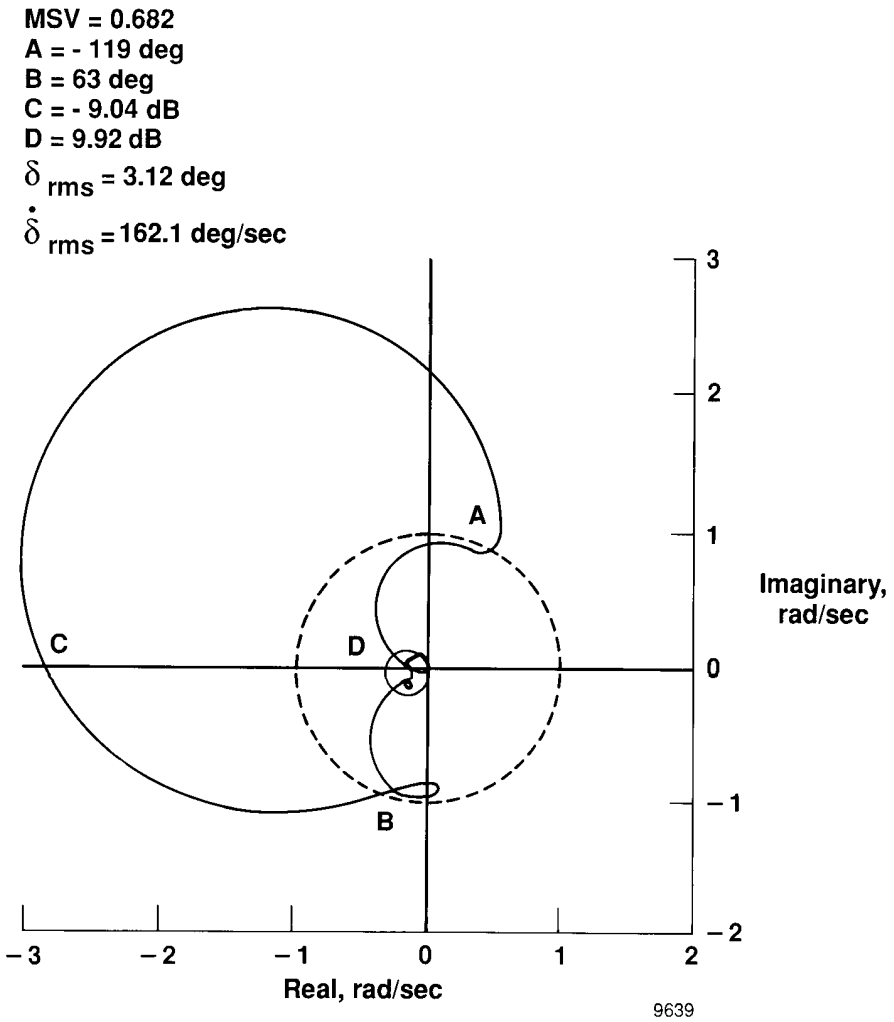

Figure 19. Nyquist plot at Q = 124 lb/ft^2 of aerodynamic energy control law A5. Optimized at Q_D = 142.6 lb/ft^2, with actuator and structural filter using inboard accelerometer.

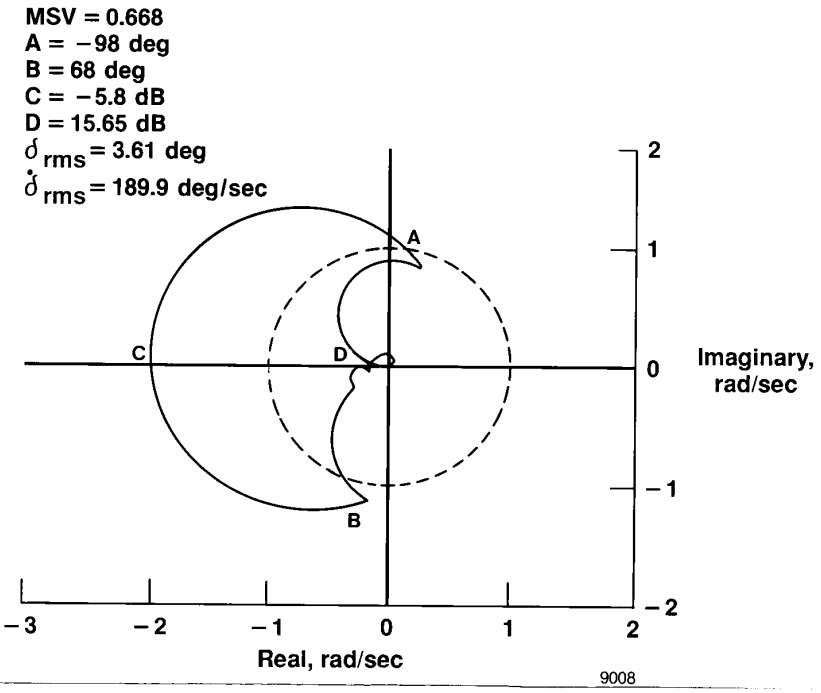

Figure 20. Nyquist plot at Q = 134 lb/ft^2 of aerodynamic energy control law B5. Optimized at Q_D = 142.6 lb/ft^2, with actuator and structural filter using outboard accelerometer.

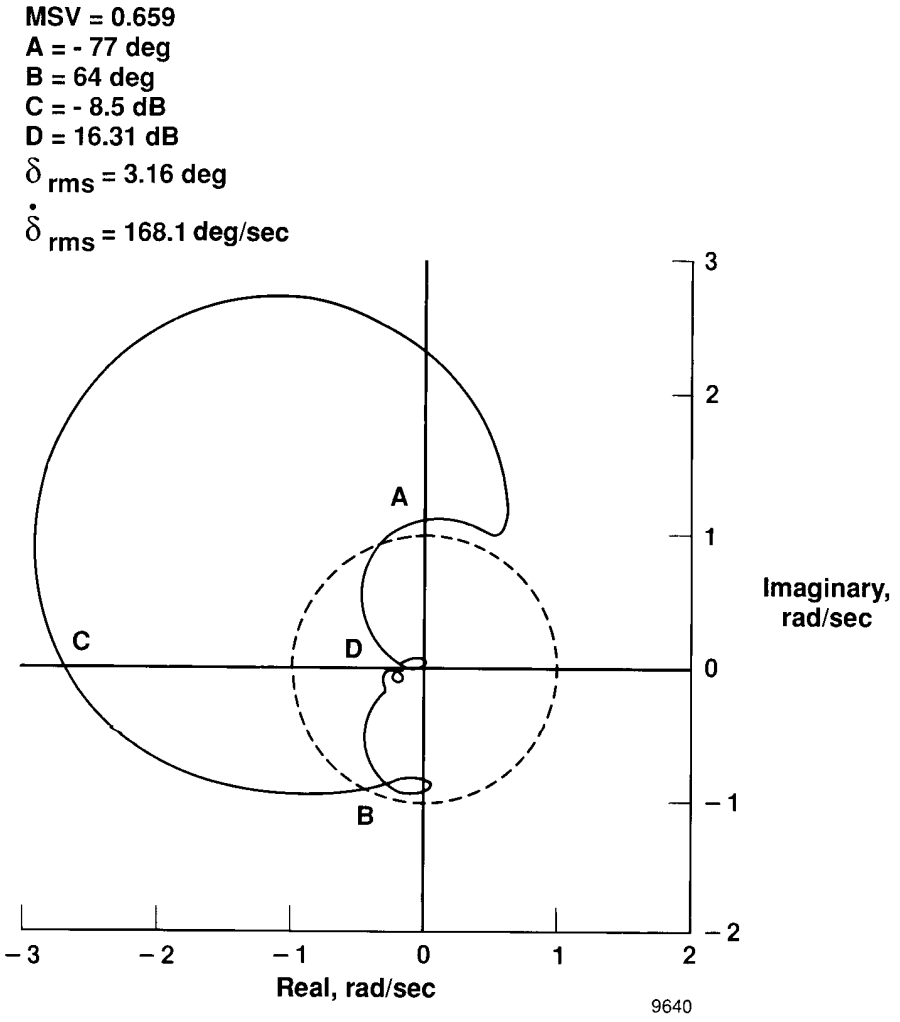

Figure 21. Nyquist plot at Q = 124 lb/ft^2 of aerodynamic energy control law B5. Optimized at Q_D = 142.6 lb/ft^2, with actuator and structural filter using outboard accelerometer.

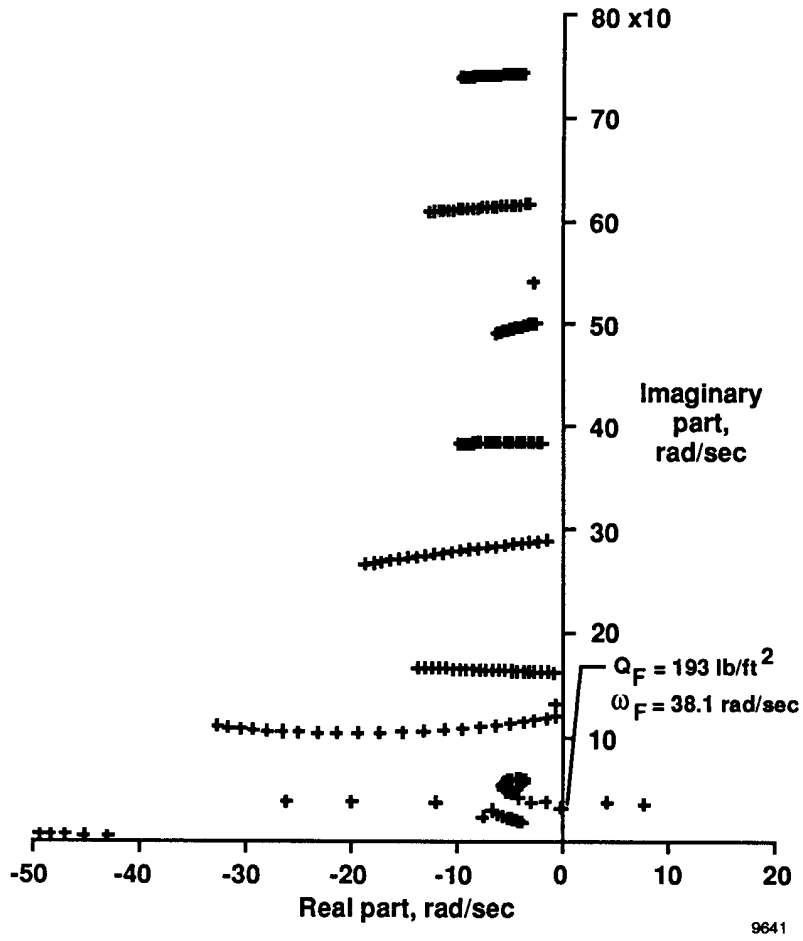

Figure 22. Closed-loop root locus plot using aerodynamic energy control law A5. Optimized at Q_D = 142.6 lb/ft^2, with actuator and with structural filter at W_s = 1000, $\underline{\sigma}_D$ = 0.9, and $\omega_{n_T} \geq 20$ using inboard accelerometer.

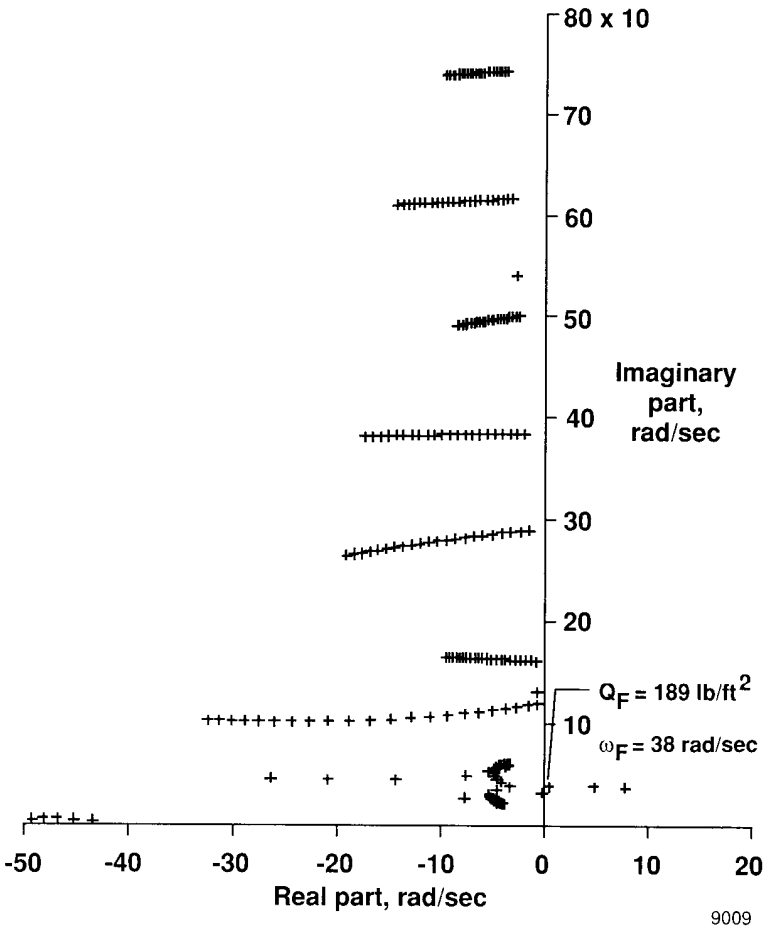

Figure 23. Root locus plot using aerodynamic energy control law B5. Optimized at Q_D = 142.6 lb/ft^2, with actuator and structural filter at W_s = 1000, ς_D = 0.85, and $\omega_{n,T} \geq 25$ using outboard accelerometer.

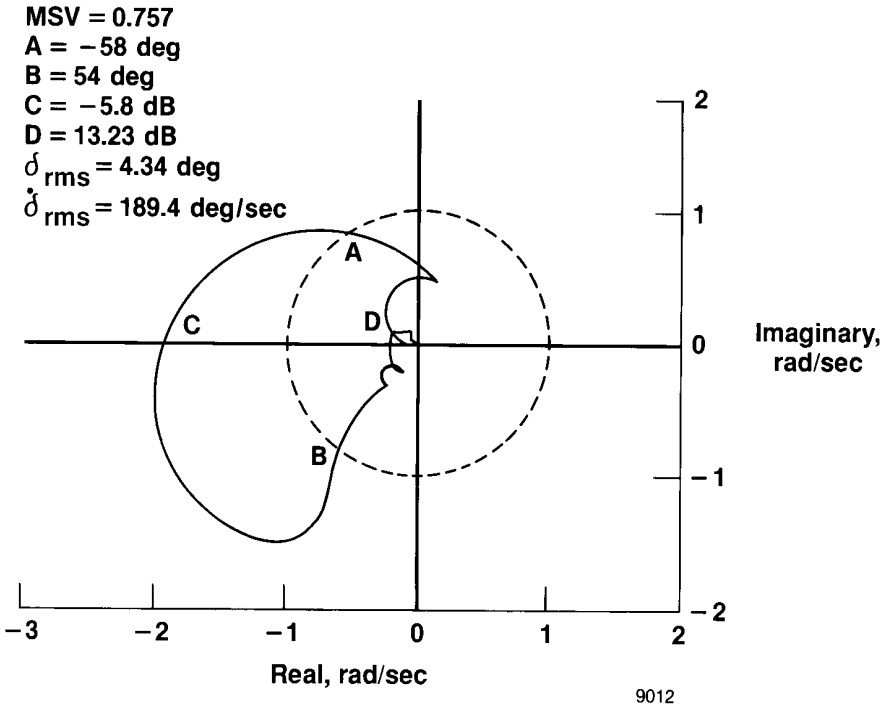

Figure 24. Nyquist plot at Q_D = 151 lb/ft^2 using aerodynamic energy control law B7. Optimized with actuator but without structural filter at Q_D = 151 lb/ft^2, with W_s = 1000 and ζ_D = 1 using outboard accelerometer.

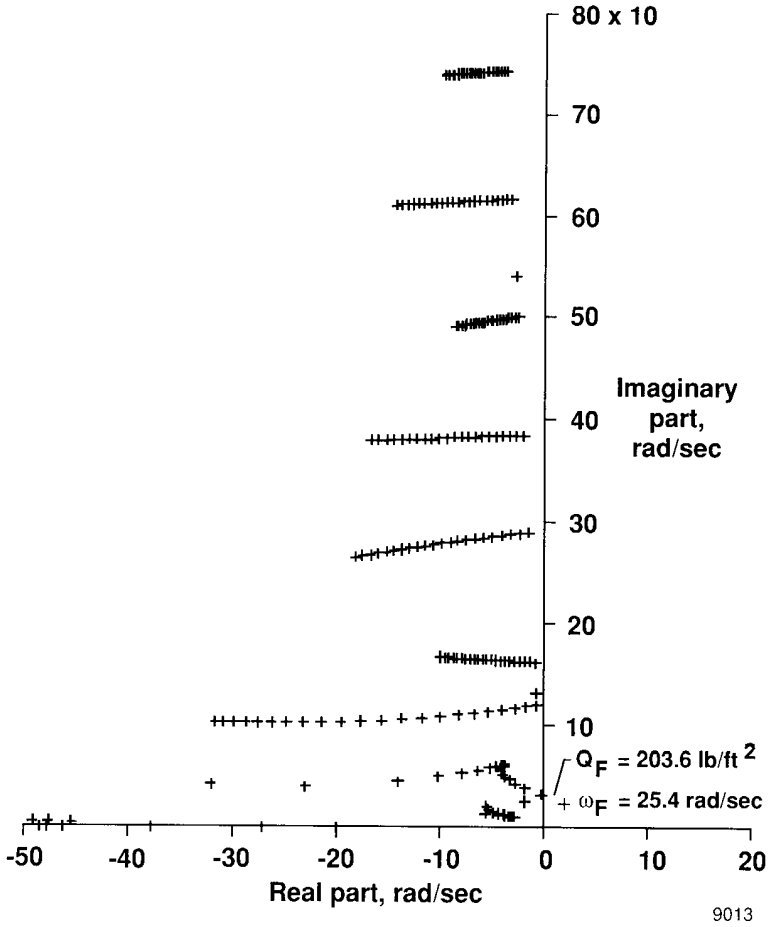

Figure 25. Closed-loop root locus plot using aerodynamic energy control law B8. Optimized at Q_D = 151 lb/ft^2, with actuator but without structural filter using outboard accelerometer.

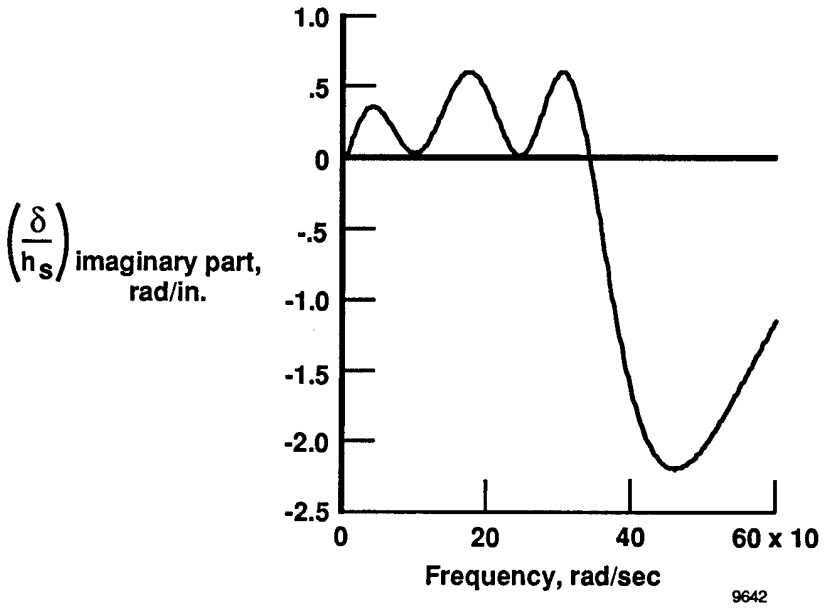

(a) Imaginary part.

Figure 26. Real and imaginary parts of control deflection per unit displacement of outboard sensor using control law given by equation (9), Newsom et al. (1980).

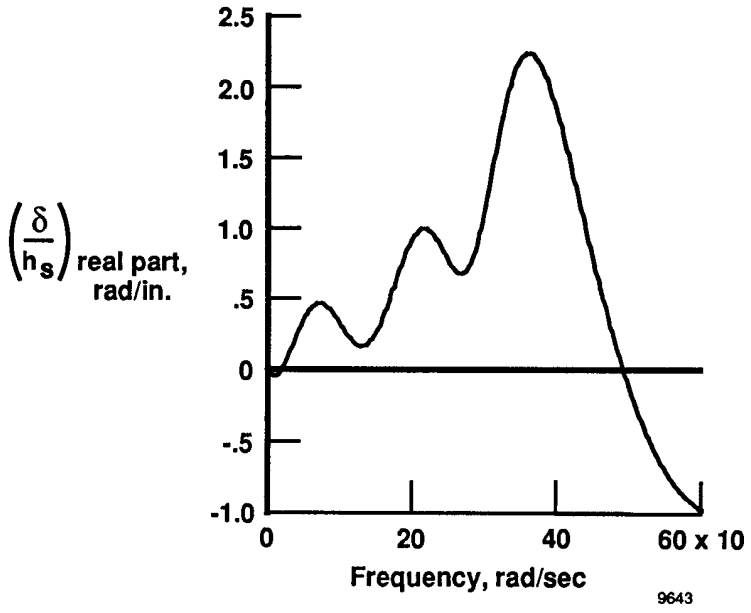

(b) Real part.

Figure 26 Concluded.

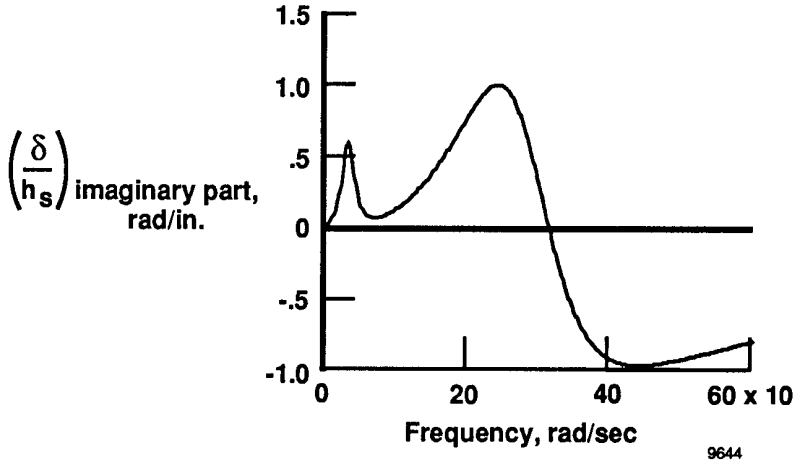

(a) Imaginary part.

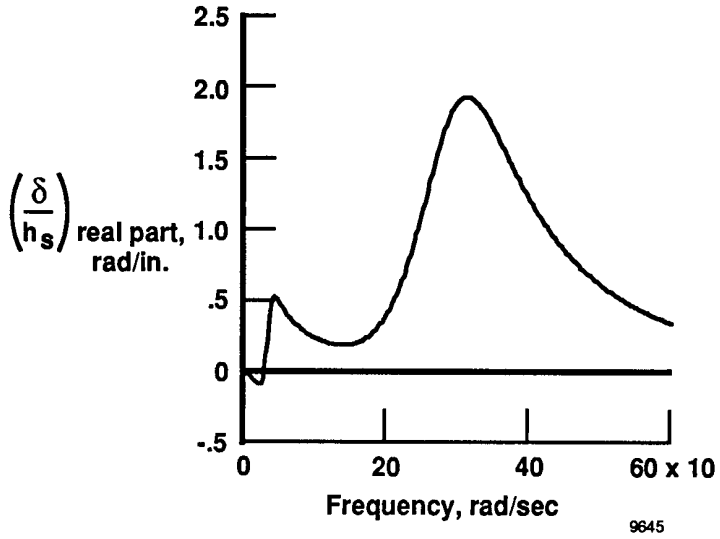

(b) Real part.

Figure 27. Real and imaginary parts of control deflection per unit displacement of outboard sensor using control law given by equation (30), Mukhopadhyay et al. (1981).

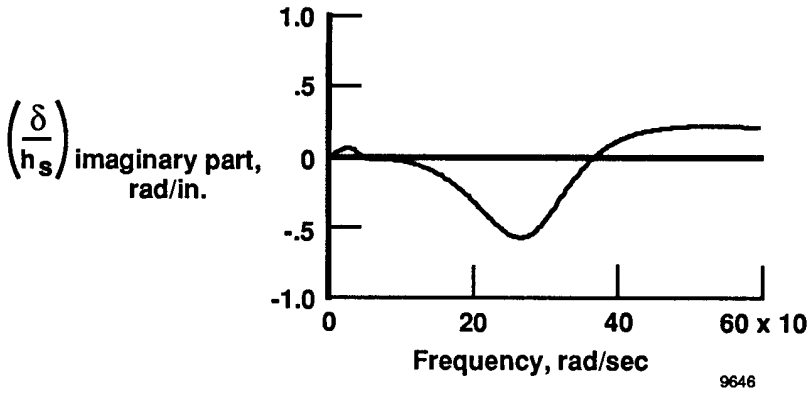

(a) Imaginary part.

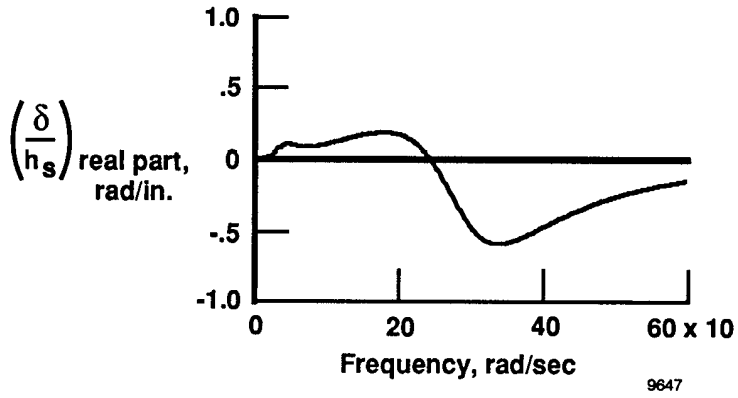

(b) Real part.

Figure 28. Real and imaginary parts of control deflection per unit displacement of outboard sensor using control law given by equation (29), Mukhopadhyay et al. (1981).

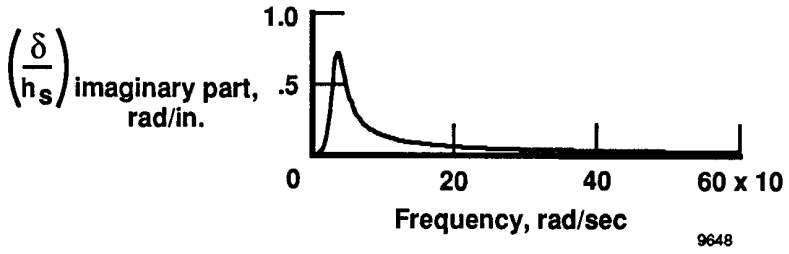

(a) Imaginary part.

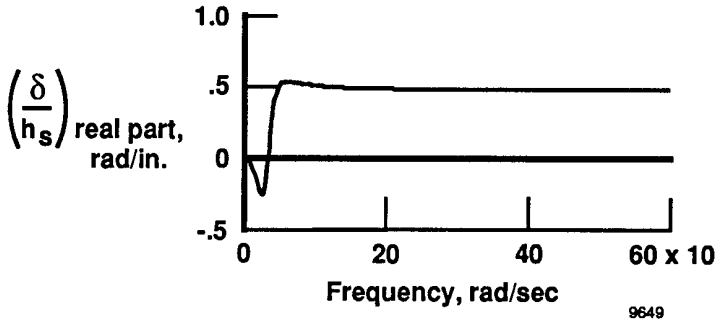

(b) Real part.

Figure 29. Real and imaginary parts of control deflection per unit displacement of inboard sensor using control law A3 with no actuator.

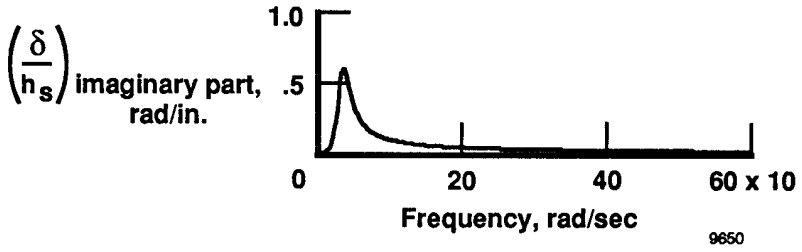

(a) Imaginary part.

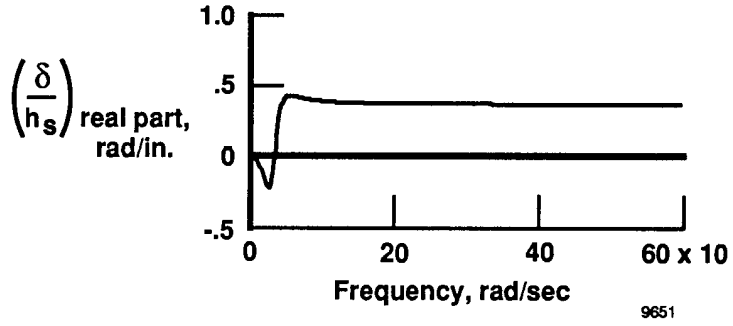

(b) Real part.

Figure 30. Real and imaginary parts of control deflection per unit displacement of outboard sensor using control law B3 with no actuator.

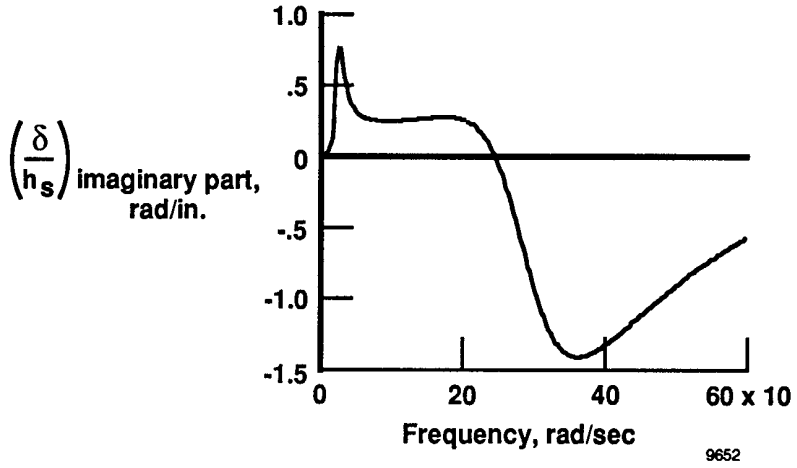

(a) Imaginary part.

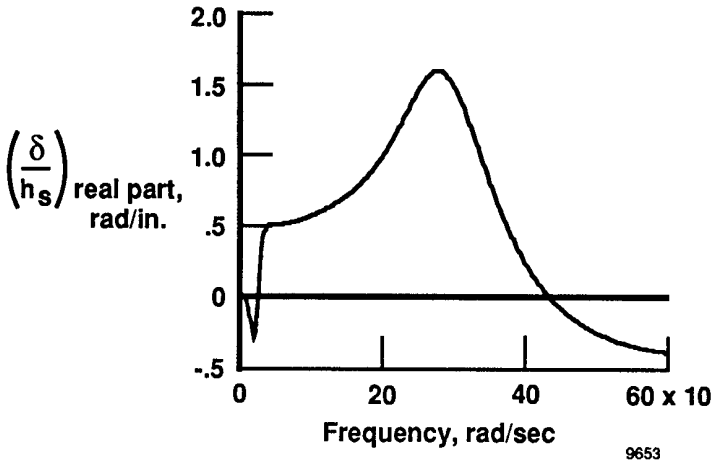

(b) Real part.

Figure 31. Real and imaginary parts of control deflection per unit displacement of inboard sensor using control law A5. Optimized with actuator and with structural filter.

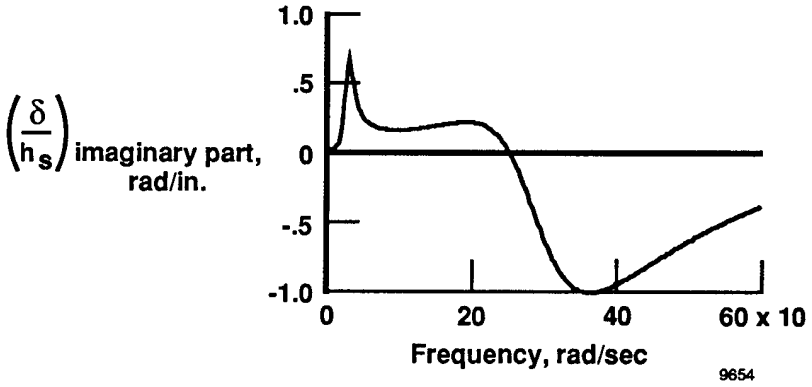

(a) Imaginary part.

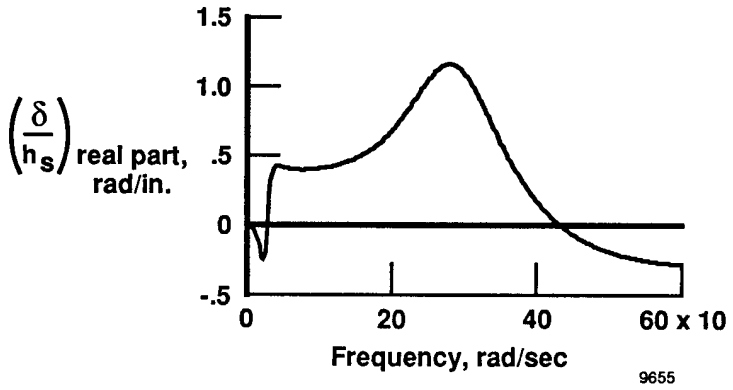

(b) Real part.

Figure 32. Real and imaginary parts of control deflection per unit displacement of outboard sensor using control law B5. Optimized with actuator and with structural filter.

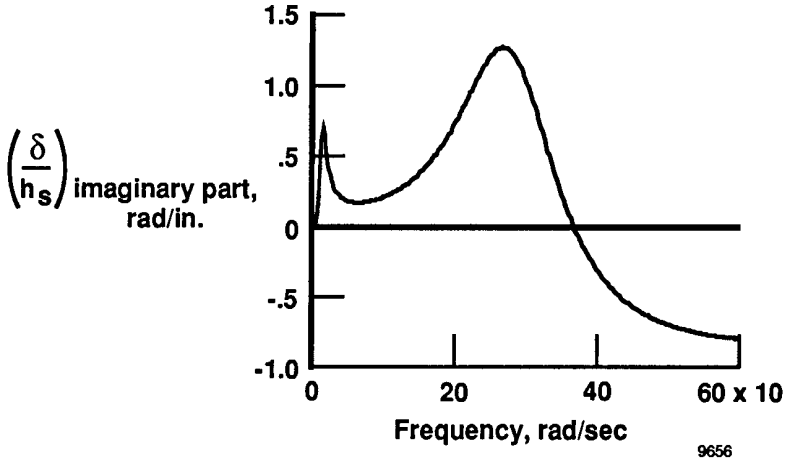

(a) Imaginary part.

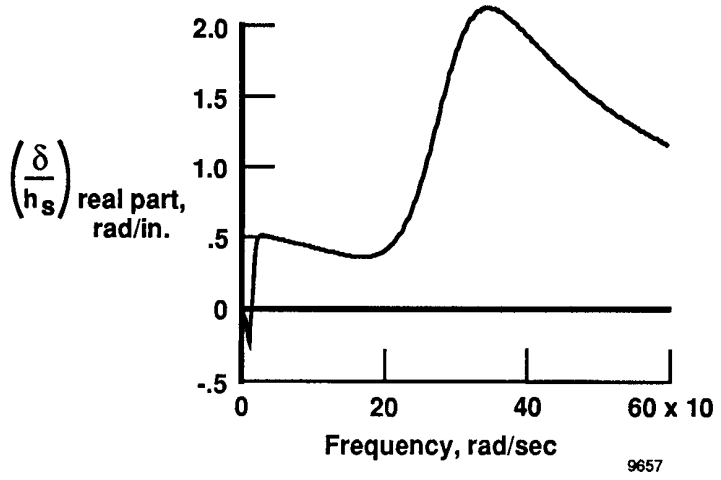

(b) Real part.

Figure 33. Real and imaginary parts of control deflection per unit displacement of outboard sensor using control law B7. Optimized at Q_D = 151 lb/ft^2, with actuator but without structural filter.

NASA
National Aeronautics and Space Administration

Report Documentation Page

1. Report No.	2. Government Accession No.	3. Recipient's Catalog No.
NASA TP-3056		

4. Title and Subtitle

Design of Control Laws for Flutter Suppression Based on the Aerodynamic Energy Concept and Comparisons With Other Design Methods

5. Report Date

October 1990

6. Performing Organization Code

7. Author(s)

E. Nissim

8. Performing Organization Report No.

H-1549

10. Work Unit No.

RTOP 505-66-71

9. Performing Organization Name and Address

NASA Ames Research Center
Dryden Flight Research Facility
P.O. Box 273, Edwards, California 93523-0273

11. Contract or Grant No.

13. Type of Report and Period Covered

Technical Paper

12. Sponsoring Agency Name and Address

National Aeronautics and Space Administration
Washington, DC 20546-3191

14. Sponsoring Agency Code

15. Supplementary Notes

This research was undertaken while Eli Nissim held a National Research Council–NASA (Ames Research Center, Dryden Flight Research Facility) Research Associateship. The author was on leave from Technion–Israel Institute of Technology. A part of this report was presented as AIAA-89-1212.

16. Abstract

The aerodynamic energy method is used to synthesize control laws for NASA's drone for aerodynamic and structural testing–aerodynamic research wing 1 (DAST–ARW1) mathematical model. The performance of these control laws in terms of closed-loop flutter dynamic pressure, control surface activity, and robustness is compared with other control laws that appear in the literature and that relate to the same model. A control law synthesis technique that makes use of the return difference singular values is developed in the present work. It is based on the aerodynamic energy approach and is shown to yield results that are superior to those results given in the literature and are based on optimal control theory. Nyquist plots are presented, together with a short discussion regarding the relative merits of the minimum singular value as a measure of robustness as compared with the more traditional measure involving phase and gain margins.

17. Key Words (Suggested by Author(s))

Active controls
Aeroservoelasticity
Flutter suppression

18. Distribution Statement

Unclassified — Unlimited

Subject category 39

19. Security Classif. (of this report)	20. Security Classif. (of this page)	21. No. of pages	22. Price
Unclassified	Unclassified	59	A04

NASA FORM 1626 OCT 86

**For sale by the National Technical Information Service, Springfield, VA 22161-2171.*

NASA-Langley, 1990